Late Miocene proboscideans from Samos Island (Greece) revisited: New specimens from old collections

George E. Konidaris[1, *], George D. Koufos[2]

[1] Eberhard-Karls University of Tübingen, Palaeoanthropology, Senckenberg Centre for Human Evolution and Palaeoenvironment, Rümelinstr. 23, 72070 Tübingen, Germany

[2] Aristotle University of Thessaloniki, Department of Geology, Laboratory of Geology and Palaeontology, 54124 Thessaloniki, Greece

[*] Corresponding author. E-mail address: geo.konidaris@gmail.com (G. Konidaris)

ORCID: 0000-0002-7041-233X

Abstract

In this article we present new proboscidean remains from the late Miocene (Turolian) of Samos Island (Greece), which are stored at the old Samos collections of Darmstadt, Frankfurt a. M. (Germany), Lausanne (Switzerland) and Vienna (Austria), and originate from the excavations or fossil collections that took place on the island at the end of the 19th and the beginning of the 20th century. The specimens belong to juvenile individuals of deinotheres, choerolophodonts and amebelodonts. The deinothere material is attributed to the last European huge-sized deinothere, *Deinotherium proavum*. The described skull from Samos is so far the most complete specimen of all known Miocene juvenile deinotheres from Eurasia and Africa. The majority of the Samos choerolophodont specimens represent the advanced morph of *Choerolophodon pentelici*, whereas one shows more archaic features and belongs to the primitive evolutionary stage of this species. This more primitive morph could originate from the lower fossiliferous horizons of Samos, which are dated to the early Turolian. The third proboscidean is attributed to the tetralophodont shovel-tusker *Konobelodon atticus*, a rare taxon in the Samos fauna. Together with the previously described zygodont *Mammut* from Samos, these four proboscideans are typical for the Turolian proboscidean fauna of Southeastern Europe. We discuss the biostratigraphy of the Samos proboscideans aiming to unravel some aspects of the chronological range of the late Miocene proboscideans with emphasis in the Southern Balkans and Turkey.

Keywords Proboscidea, *Deinotherium*, *Choerolophodon*, *Konobelodon*, biostratigraphy, Turolian

Introduction

The presence of proboscideans in the late Miocene of Samos Island (Aegean Sea, Greece, Fig. 1) was recognized since the first excavations in the Mytilinii Basin in 1887 and 1889 (Forsyth-Major 1888, 1894). Later on, several scientists and fossil dealers collected numerous fossil vertebrates from Samos, including several proboscidean specimens, which were subsequently dispersed into various museums and institutions across Europe and the U.S.A, where they are stored today. Apart from the classic monographs of Schlesinger (1917, 1922), which include the Samos choerolophodonts stored at the collections of Vienna (Austria) and Budapest (Hungary), proboscideans were not studied in detail and as a whole. Recently, new investigations on the Samos proboscideans started aiming for an updated taxonomic and biostratigraphic study, including specimens from the various old collections, as well as those from the new excavations carried out on the island (Konidaris 2013; Konidaris and Koufos 2009, 2013). In this article, we present further and important specimens that were studied during the last years in the old Samos collections of Darmstadt, Frankfurt a. M. (Germany), Lausanne (Switzerland) and Vienna (Austria). Detailed information on the stratigraphy, the old and new localities, the mammal fossils, the age and the palaeoecology of the Samos faunas are given in Koufos and Nagel (2009).

Materials and methods

The studied material includes so far unpublished specimens from the old Samos collections stored at HLMD, MGL, NHMW and SMF. The MGL and NHMW material was included in the study of Konidaris (2013) and briefly discussed in Konidaris and Koufos (2013), but here is studied in detail. The MGL proboscideans derive from the excavations of Forsyth-Major (1888, 1894) in "Andriano", corresponding to the Adrianos ravine, i.e, the main fossiliferous region of the Mytilinii Basin. The studied NHMW specimen is not included in the

study of Schlesinger (1917); it could have been purchased from K. Acker (who collected material from all Samos localities during 1909–1920), like the choerolophodont crania stored at NHMW. The HLMD specimen (acquired by the museum in 1920) could have been collected either by K. Acker or B. Sturtz, who commissioned K. von Borne to excavate in Samos during 1889–1900 (Solounias 1981). This could be also the case for the SMF specimens, for which the only information given is that they are part of the acquired Korff's collection; these specimens were mentioned and figured in an article for the public (Drevermann 1930).

Comparative material has been studied at AMPG, GPIH, FSL, HGI, ML, MNHN, NHMW, SNSB-BSPG and SU. The deinothere dental terminology follows Pickford and Pourabrishami (2013) and is shown in Fig. 3a–b, and the choerolophodont one is according to Tassy (1996a). For the cheek teeth, the metric parameters measured are the maximal mesiodistal diameter (length) and the maximal labiolingual diameter (width). The measurements were taken with digital calipers or in the case of large cranial and mandibular measurements with a measuring tape; those in brackets indicate the greatest measurable value of a parameter in incomplete or inadequately preserved specimens. Cranial and mandibular measurements follow Tassy (1996b). All measurements are given in Tables 1–3.

Institutional abbreviations

AMPG, Athens Museum of Palaeontology and Geology, National and Kapodistrian University of Athens (Greece); **FSL,** Faculté des Sciences de Lyon (France); **GPIH,** Geologisch-Paläontologisches Institut, Hamburg (Germany); **HGI,** Hungarian Geological Institute (Budapest); **HLMD,** Hessisches Landesmuseum Darmstadt (Germany); **LGPUT,** Laboratory of Geology and Palaeontology, Aristotle University of Thessaloniki (Greece); **MGL,** Musée Cantonal de Géologie, Lausanne (Switzerland); **ML,** Musée des Confluences, Lyon (France); **MNHN,** Muséum National d'Histoire Naturelle (Paris, France); **NHMA,** Natural History Museum of the Aegean, Mytilinii (Samos Island, Greece); **NHMW,** Naturhistorisches Museum

Wien (Austria); **SMF,** Senckenberg Museum Frankfurt a. M. (Germany); **SNSB-BSPG,** Staatliche Naturwissenschaftliche Sammlungen Bayerns-Bayerische Staatssammlung für Paläontologie und Geologie, München (Germany); **SU,** Palaeontology Museum of the Sofia University (Bulgaria).

Dental abbreviations: aprcc2, anterior pretrite central conule of the second loph(id); **DP,** upper deciduous premolar; **dp,** lower deciduous premolar; **pprcc1,** posterior pretrite central conule of the first lophid.

Systematic palaeontology

Class **Mammalia** Linnaeus, 1758

Order **Proboscidea** Illiger, 1811

Superfamily **Deinotherioidea** Osborn, 1921

Family **Deinotheriidae** Bonaparte, 1845

Genus ***Deinotherium*** Kaup, 1829

Deinotherium proavum (Eichwald, 1831)

Material: partial cranium with the DP2–DP4 of both sides and associated mandible with the dp2–dp4 of both sides, SMF-M 3604; right mandibular fragment with partial lower tusk and the dp3–dp4, MGL-S 1048 / S 380; left mandibular fragment with the dp4, MGL-S 381 [the MGL specimens originate from "Andriano"; MGL-S 380 and S 381 were attributed to "*Mastodon turicensis*" by Forsyth Major (1894)].

Description: The cranium SMF-M 3604 is strongly deformed and damaged (Fig. 2a–d). Several parts are missing, including the rostral part of the cranium with the nasal aperture and the premaxilla, the right side of the basicranium, both zygomatic arches, and most of the occipital except of the right supraoccipital and the fossa for the insertion of the nuchal ligament.

In ventral view (Fig. 2c), the palate with both complete deciduous tooth rows is well preserved. The distal end of the tooth rows is aligned with the front border of the choanae. The anterior zygomatic process is situated at the level of the distal part of the DP3 and the mesial part of the DP4. In lateral view (Fig. 2a), the infraorbital foramen lies above the first loph of the DP3 and the orbit above the DP4. The temporal fossa is partially preserved and rather deep. In dorsal view (Fig. 2b), the right side of the neurocranium is relatively well preserved, having almost quadrangular shape. The distal parietal border with the occipital is rather straight. The coronal and frontonasal sutures are partly visible; they are not fully fused, in accordance with the juvenile age of the individual. The nasal bone is damaged at the level of the nasal process. In occipital view (Fig. 2d), the right part of the supraoccipital bone is preserved, as well as the fossa for the insertion of the nuchal ligament, which is located towards the top of the cranium.

The associated mandible SMF-M 3604 (Fig. 2e–f) preserves the mandibular corpus including most of the symphysis (missing lower tusks), the complete deciduous dentition, as well as most of the ramus except of the coronoid process and the mandibular condyle. The mandible MGL-S 1048 / S 380 (Fig. 2g–h) preserves most of the corpus with the proximal part of the lower tusk, the dp2 alveolus, the dp3, and the erupting dp4. In both specimens, the symphysis is strong and ventrally deflected. The dorsal ridge of the symphysis is deflected downwards, ~38° and ~25° relative to the alveolar planum in SMF-M 3604 and MGL-S 1048, respectively. The posterior mental foramen is located almost at the level of the mesial border of the dp2. The corpus forms an obtuse angle with the ramus measured ventrally ~145° in SMF-M 3604. The region of the mandibular angle in the latter specimen is well developed.

The DP2 is bilophodont (Figs. 3a, 4o). It bears a mesial cingulum, stronger and more pointed at the mesiolabial side, consisting of numerous conelets and a distinct parastyle; more labially to the parastyle there is one additional lower, but rather strong conelet. The cingulum continues towards the lingual side of the tooth with weaker conelets until the lingual side of the protocone and it faints at the lingual wall of the hypocone. The proto- and paracone are

connected by a worn and low transverse ridge; the proto- and hypocone are well separated by an open valley. The hypocone bears a ridge of conelets towards the labial side, but it is not connected to the metacone. In the ectoloph, the para- and metacone are connected by worn conelets, with only a weak interruption at the middle. Distally to the metacone several more conelets diminish in height forming the distal end of the ectoloph and connect with the distal cingulum.

The DP3 consists of two lophs clearly separated by an open transverse valley (Fig. 3a). There is a developed mesial cingulum, where the strong parastyle is connected to the weaker protostyle by a worn ridge. A weak ridge connects labially the parastyle and the paracone. The proto- and paracone, and the hypo- and metacone, are connected by slightly mesially curved crests, forming the fairly worn protoloph and the only slightly worn metaloph. The ectoflexus is clearly marked. The postparacrista and postmetacrista are well developed, whereas the postprotocrista is weaker. The distal cingulum is low with a strong metastyle.

The DP4 is trilophodont (Fig. 3a). The mesial cingulum is rather low, but the parastyle is strong; a weak ridge connects the latter with the paracone. Slightly mesially curved crests consisting of numerous conelets connect the main cusps of each loph and form the proto-, meta- and tritoloph. Both the ectoflexus are pronounced. The postparacrista and postmetacrista are strong, but the postmetacrista weaker. The distal cingulum is low and weak.

The dp2 has a triangular shape (Figs. 3b, 4i). A rudimentary mesial cingulum is present at the mesio-lingual side and is connected through a weak paracristid to the protoconid. The narrow and high mesial part is comprised of the strong proto- and metaconid; the latter is even more robust. These two cuspids are fused, however, their rounded apices are clearly distinct. The protoconid is set mesially to the metaconid, which is connected with the hypolophid by the ectolophid. An open valley separates clearly the metaconid from the entoconid. A weak crest connects the ento- and hypoconid forming the hypolophid.

The dp3 is bilophodont with wider hypolophid (Fig. 3b). The mesial cingulum is strong and projecting slightly mesially at the labial side. It is connected through the preprotocristid (paracristid) with the protoconid. A worn and distally curved crest connects the proto- and metaconid. The transverse valley is open. The hypolophid is less worn and less curved. The prehypocristid (cristid obliqua) is rather strong. The distal cingulum is relatively low and formed by numerous conelets.

The dp4 is trilophodont (Fig. 3b–c). The mesial cingulum is low and more developed at the labial side. The preprotocristid is stronger than the other cristids (in the MGL specimen also the prehypocristid). The crests that connect in each lophid the main cuspids are rather straight. The distal cingulum is low and straight.

Remarks: Based on several dental, cranial and postcranial features, European deinotheres are represented by the early–middle Miocene *Prodeinotherium* and the middle–late Miocene *Deinotherium*. Five species are considered here valid: *P. cuvieri* (Kaup, 1832) from the early–middle Orleanian, *P. bavaricum* (von Meyer, 1831) from the late Orleanian–early Astaracian, *D. levius* Jourdan, 1861 from the late Astaracian, *D. giganteum* Kaup, 1829 from the Vallesian and *D. proavum* (Eichwald, 1831) (= *D. gigantissimum* Stefanescu, 1892) from the Turolian. Distinctive features among the species include: a) dental dimensions, b) traits of the mandible (shape of the symphysis and the mandibular angle), and c) the morphology of the p3 and the dp2/DP2 [see below; for further details on the taxonomy of European deinotheres see Aiglstorfer et al. (2014), Konidaris et al. (2017) and references cited in both].

In contrast to the conservative dental morphology throughout the evolutionary history of deinotheres, the dental dimensions increased progressively from the early to the late Miocene in the previously defined European species. The metrical comparison of the Samos deciduous teeth (Fig. 4a) shows that they are clearly distinguished from the two *Prodeinotherium* species from several middle Orleanian–early Astaracian (MN 4–MN 6) French and German localities, as well as from *D. levius* from the late Astaracian (MN 7/8) localities La Grive (France) and

Massenhausen (Germany). Both the MGL and SMF Samos specimens surpass also the *D. giganteum* sample from Montredon (France, late Vallesian, MN 10) and are plotted among the upper range of *D. proavum* dimensions from several localities (Fig. 4a). The teeth from Samos are the largest ones known so far permitting their attribution to this species.

Konidaris et al. (2017) noted that the morphology of the dp2 differs among the European deinotheriid species. In *P. cuvieri* from Montréal-du-Gers (Fig. 4b) the proto- and metaconid are clearly separated, in *D. levius* from La Grive (ML-LGR 893, LGR 900, LGR 959; Ginsburg and Chevrier 2001: fig. 7) and in *D. giganteum* from Montredon (ML-MR- 52, FSL-210393) these cusps are either connected or almost/totally fused. In all of the above mentioned species the ectolophid is connected with the protoconid (Fig. 4b–e). On the other side, in *D. proavum* from Pikermi (AMPG-PA3950/91) the ectolophid is connected with the metaconid, and thus it is placed more oblique (~33°) relative to the long axis of the tooth (Fig. 4h). This morphology is also present in the dp2s SMF-M 3604 from Samos (Fig. 4i) further corroborating its possible taxonomic value. If this is confirmed in the future by more specimens, the Nessebar (Bulgaria; Bakalow 1914; Bakalov and Nikolov 1962) and Kayadibi (Turkey; Gaziry 1976) juvenile specimens (Fig. 4f–g) attributed to *D. proavum* based on their dimensions (Markov 2004, 2008; Konidaris et al. 2017), would fit better with an attribution to *D. giganteum*, as they are morphologically different from Pikermi and Samos, and more similar to FSL-210393 of *D. giganteum* from Montredon (Fig. 4e). The dimensions of their lower deciduous teeth are similar and indeed large (but see the smaller upper deciduous teeth from Nessebar), however, not much larger than the Montredon ones (Fig. 4a), so that an attribution to this species would be plausible, taking also into account the unknown size variability of *D. giganteum* due to the limited specimens. Nessebar is correlated to the Vallesian (Spassov and Koufos 2002) and thus the presence of the Vallesian *D. giganteum* would fit well with the rest of the fauna. Kayadibi is usually correlated to the early Turolian; nonetheless Konidaris et al. (2016) based on the presence of the Vallesian *Choerolophodon anatolicus* questioned the Turolian age. If the

Kayadibi deinothere belongs indeed to *D. giganteum*, this would further indicate a Vallesian age for this locality, in accordance with the evolutionary stage of the choerolophodonts. In any case more material is certainly needed to shed light on this issue. Interestingly, however, is that the connection of the ectolophid with the metaconid is present in the dp2 of the African *Deinotherium bozasi* from the Pliocene of Laetoli (Tanzania; Harris 1987).

The DP2 presents also some morphological differences among the European deinotheriid taxa. In *Prodeinotherium* from Tavers, Pontlevoy (France) and Esselborn (HLMD-Din 237; Germany) the DP2 has triangular shape, as the protoloph is much narrower than the metaloph, and the proto- and paracone are rather close located; these cusps are connected through a strongly curved crest (Fig. 4j–k; Stehlin 1925: fig. 21b). Moreover, the mesial projection of the mesial cingulum is relatively weak. Although the sample is limited, these morphological features seem to differentiate the DP2s of *Prodeinotherium* and *Deinotherium*. In *D. levius* from La Grive and Massenhausen, the crest connecting the protocone and paracone is also curved, but these cusps are more distant to each other, giving a more trapezoid shape to the tooth (widening of the protoloph), and the mesial projection of the mesial cingulum is prominent (Fig. 4l–m). In *D. giganteum* and *D. proavum* the crest is less curved than *D. levius*, resulting in the more L-shaped connection of the proto- and ectoloph (Fig. 4n–o; see also Gaziry 1976; Sanders 2003; Garevski and Markov 2011). Following the two European deinothere species concept (*P. bavaricum-D. giganteum*) of Huttunen (2002), Göhlich and Huttunen (2009: pl. 1, fig. 1) attributed a DP2 from Atzelsdorf (Austria) to *Deinotherium giganteum*. Accepting here the validity of *D. levius* and according to the above comparison, this tooth is closer morphologically and metrically to ML-LGR 970 of *D. levius* from La Grive (Fig. 4a, l) rather than to FSL-210255 and 210239 of *D. giganteum* from Montredon (Fig. 4n). Taking also into account the dimensions of the P3 from Atzelsdorf, an attribution to *D. levius* seems plausible. This possible occurrence of the late Astaracian (MN 7/8) *D. levius* in the lowermost

Vallesian (earliest MN 9) of Atzelsdorf is not so surprising, considering also the presence in the fauna of the primitive brachyodont equid *Anchitherium* (Daxner-Höck and Göhlich 2009).

No other cranium of a juvenile deinothere is known in Europe. The only comparable, but still unpublished specimen, is a cranium of *Prodeinotherium* from the early Miocene of Langenau (Germany), illustrated in Heizmann et al. (1996). Apart from this, there is the palate of *D. proavum* from Kiro Kucuk (Garevski and Markov 2011). SMF-M 3604 shares with this specimen: a) the distal end of the tooth rows is aligned with the front border of the choanae, b) the anterior root of the zygomatic process is located at the level of the distal part of the DP3 and the mesial part of the DP4, and c) the infraorbital foramen lies above the first loph of the DP3. Concerning the mandible, the mandibular angle in the Samos specimen is well developed, but does not extend the ventral border of the corpus (Fig. 2e), as it is observed in adult mandibles of *D. proavum* (Tarabukin 1974; Markov 2008); however, the ontogenetic development of this character is unknown in deinotheres. In this trait, it is similar to the Nessebar mandible SU-191 and different from the weaker one of the slightly older in ontogenetic age mandible from Isle-en-Dodon (MN 7, France; Lartet 1859: pl. 13, fig. 4; Duranthon et al. 2007).

Superfamily **Elephantoidea** Gray, 1821

Family **Gomphotheriidae** Hay, 1922

Subfamily **Choerolophodontinae** Gaziry, 1976

Genus ***Choerolophodon*** Schlesinger, 1917

Choerolophodon pentelici (Gaudry and Lartet, 1856)

Material: partial cranium with the erupting DP4s of both sides and associated right hemimandible with the dp3 and the erupting dp4, SMF-M 3603; right DP2, MGL-S 614; maxilla with the DP3–DP4 of both sides, HLMD-SS 230; right and left mandibular fragments with the dp3s, MGL-S 340; right mandibular fragment with dp4 and associated fragment with

distal part of m1, and left mandibular fragment with dp4 and partial m1, MGL-S 333 (the MGL specimens originate from "Andriano").

Description:

The juvenile cranium SMF-M 3603 (Fig. 5a–d) preserves its front part until the frontal bone on the dorsal side and until the left glenoid fossa on the ventral side; the right zygomatic arch, and the whole caudal part of the cranium (partial basicranium, and the parietal and occipital bones) are missing, as are also the DP2 and DP3 on both sides, whose alveoli are visible. The facial region is moderately inclined (Fig. 5d). The almost circular orbit is situated well behind the DP4, the postorbital process of the frontal is strong and the orbitotemporal crest runs downwards and anteriorly. The anterior root of the zygomatic process is located above the erupting DP4 in lateral view and at the level of the anterior border of the choanae in ventral view (Fig. 5b, d); the preserved right zygomatic arch is only slightly flaring from the cranium. On the dorsal side, the frontal is relatively flat, the nasal fossa is narrow and the rather elongated premaxillae bear the still in alveolus right and left upper tusks (Fig. 5a). Caudally, the mesial part of the brain cavity is visible, where the olfactory bulbs are attached (Fig. 5c). Associated to the cranium is the right hemimandible; it lacks its caudal part with the condyle (Fig. 5e–f). It preserves the much worn dp3 and the erupting dp4. The mandibular corpus forms an obtuse angle with the ramus, ~155° measured ventrally. The ventral part of the symphysis is situated horizontally at the extension of the ramus.

The DP2 MGL-S 614 is bilophodont and has a rather triangular shape; loph 1 is narrow, whereas loph 2 is wide due to its distolingual enlargement (Fig. 7). In loph 1, the proto- and paracone are appressed to each other, forming the pyramidal in shape stronger and higher part of the tooth. Loph 2 is lower, and the meta- and hypocone are clearly separated. Numerous low conelets fill the inner part of the crown. A cingulum is developed in the mesial, mesiolingual and distal side of the tooth. Cementodonty and ptychodonty are expressed.

The DP3 HLMD-SS 230 consists of two lophs with the second one being wider (Figs. 6a, 9e). The mesial cingulum and loph 1 are much worn, and the dentine is exposed almost on the entire occlusal surface. However, pretrite and posttrite half-lophs are aligned. Lophs 1 and 2 are clearly separated by ecto- and entoflexus, and a weak cingulum is developed in the labial and lingual sides of the interloph. In loph 2, the adaxial part of the pretrite half-loph is mesially offset compared to the worn hypocone and the posttrite half-loph, and connects to loph 1. The posttrite second half-loph is smaller than the pretrite one. The distal cingulum is developed and consists of several conelets. Its posttrite conelet is distinct from the metacone. The stronger pretrite one is worn, that of the right DP3 even more. Ecto- and entoflexus are not present and thus the distal cingulum does not form a third loph. Choerodonty and ptychodonty are well expressed.

The DP4 HLMD-SS 230 is trilophodont (Fig. 6a). The mesial cingulum is formed by a series of conelets. The stronger one is located in front of the protocone; an additional strong but low conelet is situated more lingually. One strong conelet is placed in front of the paracone. In loph 1, there are two posttrite mesoconelets appressed to each other but distinct from the paracone; on the pretrite side there is only one mesoconelet. Interloph 1 is open labially, whereas lingually there is one strong aprcc2, blocking the transverse valley. A relatively strong cingulum is located in the lingual sides of both interlophs 1 and 2. In loph 2, a series of posttrite mesoconelets are appressed to each other and the metacone, whereas one strong and distinct mesoconelet is located at the pretrite side. In loph 3, the more mesial position of the mesoconelets compared to the main cusps, results in a chevron structure. The distal cingulum consists by a series of conelets increasing in size and height towards the lingual side, where it connects to the pretrite main cusp of loph 3. Choerodonty and ptychodonty are well expressed. The DP4 SMF-M 3603 shows a similar morphology; however, the choerodonty is better expressed: one additional aprcc is located in front of the protocone, the posttrite mesoconelets of loph 1 are three, there is one additional strong conule situated distally and appressed to the

paracone, and in loph 2 the number of the mesoconelets is higher, they are more mesially located and the general structure of loph 2 is more complicated (Fig. 5b).

The dp3s MGL-S 340 are fresh and comprised of two lophids, mesial cingulum and a much developed distal cingulum (Figs. 6b, 8f). They have a relatively elongated triangular shape, with narrow first lophid and wider second one. In lophid 1, the half-lophids are appressed to each other; each of them bears one mesoconelet. The posttrite half-lophid is distally offset from the pretrite one and connects in the interlophid through a series of conules with the aprcc2. The entoflexus 1 is marked. In lophid 2, the half-lophids are almost aligned and separated by a median sulcus. The distal cingulum is enlarged and formed by numerous conelets. It has the form of a regular lophid and is separated from lophid 2 by a second entoflexus. Second ectoflexus is absent. Choerodonty and ptychodonty are well expressed. The dp3 SMF-M 3603 is much worn, but shows the similar general morphology with an inflated distal cingulum (Figs. 5e–f, 8e).

The dp4 SMF-M 3603 is partially inside the alveolus and only the first two lophids are visible (Fig. 5e–f). It shows a strong mesial cingulum connected to the pretrite half-lophid 1, aligned lophid 1 and a weak chevron structure in lophid 2. In the interlophid 1 there is a strong pprcc1, whereas the aprcc2 is appressed to the mesoconelet. The dp4s MGL-S 333 are much worn and the morphology of lophid 1 is not observable (Fig. 6c). In lophid 2, the pretrite half-lophid bears one anterior and one posterior worn central conule. The latter is connected in the interlophid 2 with the aprcc3. The chevron structure is clear in lophid 3. The distal cingulum is formed by strong cusps and is connected to the pretrite main cusp of lophid 3.

Remarks: Choerolophodonts are the most common proboscideans in the late Miocene faunas of SE Europe-SW Asia, known with abundant specimens, but mostly belonging to juvenile individuals. Several taxonomic and biostratigraphic schemes have been proposed (Gaziry 1976; Tassy 1994; Sanders 2003; Konidaris et al. 2016). Based on features of the cranium, the adult mandible and the teeth, two *Choerolophodon* species are here recognized in the late Miocene:

the early Vallesian *C. anatolicus* (Ozansoy, 1965) and the late Vallesian–Turolian *C. pentelici*. *Choerolophodon pentelici* is further divided into one primitive morph from the late Vallesian–early Turolian ("*C. pentelici* primitive") and one advanced (typical) morph from the Turolian ("*C. pentelici* advanced"). The latter distinction is mainly based on the dimensions and the morphology of the dp3/DP3 [see Konidaris et al. (2016), Konidaris and Koufos (2016) and references cited in both for more details on the late Miocene choerolophodonts].

In the cranium SMF-M 3603, the position of the orbits far behind the supposedly last functional tooth (which should have been the missing DP3) and well behind the erupting DP4, the location of the anterior root of the zygomatic arch behind the dentition and at the level of the anterior margin of the choanae, and the strongly redressed perinasal area (Fig. 5), are morphological features that clearly distinguish it from the known *C. anatolicus* cranial specimens (i.e., Yassiören, Akin and Kayadibi in Turkey; Gaziry 1976: pl. 6; Konidaris and Koufos 2013: fig. 3a; Konidaris et al. 2016: fig. 7) and are shared with the approximately similar in ontogenetic ages crania of *C. pentelici* MNHN-PIK-3665 (Pikermi, Greece; lectotype,; Konidaris and Koufos 2013: fig. 2), NHMW-2014/0129/0001 (Samos; 'Cranium B' in Schlesinger 1917: pl. 23, fig. 1, pl. 24, figs. 1, 2, pl. 25, fig. 1) and HGI-Ok-548 (Samos; Schlesinger 1922: pl. 20, figs. 1, 2). No distinguishing morphological characters are known between juvenile mandibles of *C. anatolicus* and *C. pentelici*. Nonetheless, the dimensions of the mandible SMF-M 3603 (Table 2; Fig. 5e–f) are larger than the more gracile mandible of *C. anatolicus* from the type locality Yassiören (Turkey; Konidaris and Koufos 2013: fig. 3b–c) and match with those of the previously mentioned specimens of *C. pentelici* from Pikermi and Samos.

The dp3s MGL-S 340 and SMF-M 3603 are different from *C. anatolicus*, because the development of the distal cingulum is markedly stronger and the overall dimensions of the teeth clearly larger (Fig. 8). In the unworn MGL-S 340, the inflated distal cingulum has the general form of a distinct third lophid, separated from the second lophid by a second entoflexus, and

with further conelets located at the distal end of the tooth (Fig. 8f). The morphology of the MGL dp3s is different from corresponding specimens of "*C. pentelici* primitive" from Xirochori-1, Ravin de la Pluie (Axios Valley, Greece), Kemiklitepe-D (Turkey) and Kocherinovo-2 (Bulgaria) and coincides with the advanced morph of *C. pentelici* e.g., from Ravin des Zouaves-5, Nikiti-2, Pikermi, Samos (HGI, NHMW), Kemiklitepe-A (Fig. 8; Tassy 1994; Hristova et al. 2013; Konidaris et al. 2016: fig. 5). SMF-M 3603 is much worn; however, the development of the distal cingulum is similar to the lectotype of *C. pentelici* from Pikermi. Furthermore, the dimensions of the MGL and SMF dp3s are larger than "*C. pentelici* primitive" and fall into the "*C. pentelici* advanced" group (Fig. 8a). The dimensions of the dp4s MGL-S 333 are larger than those of *C. anatolicus* from Yassiören, Sinap 12 (Turkey) and Kayadibi (Gaziry 1976; Sanders 2003). The DP2 MGL-S 614 can also be allocated to the advanced morph of *C. pentelici*, because its dimensions are comfortably plotted within this group, being clearly larger than the DP2s of *C. anatolicus*, as well as of the "*C. pentelici* primitive" sample (Fig. 7).

The DP3 of the maxilla HLMD-SS 230 differs from the lectotype of *C. anatolicus* (Yassiören), displaying a more developed distal cingulum with stronger conelets, a more complicated structure due to the multiplication of the conelets, and separation of the cingulum's posttrite conelet from the metacone (Fig. 9b, e). However, it also differs from the DP3s of *C. pentelici* from the type locality (Pikermi), the other known DP3s from Samos (NHMW, HGI; Schlesinger 1917: pl. 23, fig. 1, pl. 26, fig., 1, Schlesinger 1922: pl. 20, fig. 2), as well as from Nikiti-2, Ravin des Zouaves-5, Kemiklitepe-A, B, all characterized by even more prominent distal cingulum and by presence of a slightly or strongly marked second entoflexus (Fig. 9; Konidaris et al. 2016: fig. 5). In these features HLMD-SS 230 stands closer to the DP3 LGPUT-XIR-11 and 12 of "*C. pentelici* primitive" from Xirochori-1 (Fig. 9c–d), with which it shares additionally the strongly oblique position (~60°) of the pretrite half-loph (hypocone and mesoconelet) relative to the long axis of the tooth. This morphology is so far not observed in the DP3s of "*C. pentelici* advanced" (Nikiti-2, Ravin des Zouaves-5, Dytiko-2 Pikermi,

Kemiklitepe-B and the other known DP3s from Samos), where the pretrite half-loph is either vertical or only slightly oblique relative to the long axis; however, straight pretrite half-loph may be present also in the more primitive morphs (e.g., LGPUT-XIR-23; Konidaris et al. 2016: fig. 5u). Metrically, HLMD-SS 230 is larger than the *C. anatolicus* sample and is plotted at the lower values of "*C. pentelici* advanced" and within the cluster of "*C. pentelici* primitive" (Fig. 9a). Taking into account both DP3 morphology and dimensions, HLMD-SS 230 is clearly different from *C. anatolicus* and fits better with the primitive morph of *C. pentelici*. Concerning the DP4, the dimensions of HLMD-SS 230 are larger than *C. anatolicus* (Yassiören, Kayadibi, Pentalophos-1) and within *C. pentelici* (Ozansoy 1965; Gaziry 1976; Konidaris et al. 2016).

It is worth to mention here a juvenile cranial fragment (SNSB-BSPG-1899 VII) described and illustrated by Lehmann (1950: pl. 22, fig. 109). Originally stored at the Munich collections, a direct comparison is impossible, because it was possibly destroyed during World War II. In this specimen, the DP2 is damaged, the DP3 functional and partially worn, and the DP4 in the alveolus. In agreement with the observations of Lehmann (1950), the DP3 is more primitive than other specimens, e.g., those from Samos (NHMW, HGI), Pikermi and Kemiklitepe-B, displaying weaker development of the distal cingulum. Based on the illustration, SNSB-BSPG-1899 VII appears to be morphologically close to the DP3 HLMD-SS 230; however, it is much smaller not only from this specimen, but also from those from Xirochori-1 and Ravin de la Pluie, and is placed metrically among the *C. anatolicus* sample (Fig. 9). Nonetheless, an equally small-sized, but much worn DP3 (morphology not observable) from Ravin des Zouaves-1 (late Vallesian; Axios Valley, Greece), is associated with a clear *C. pentelici* cranial morphology and it was attributed to "*C. pentelici* primitive" by Konidaris et al. (2016: fig. 6c–d). The anterior root of the zygomatic process in SNSB-BSPG-1899 VII is located behind the DP3 and at the level of the still in alveolus DP4, thus being comparable to the *C. pentelici* cranial morphology, e.g., the same in ontogentic age crania NHMW-2014/0129/0002 ["Cranium C in Schlesinger 1917: pl. 26, fig. 1)] and LGPUT-RZO-208

(Konidaris et al. 2016: fig. 6f–g). Therefore, like the skull from Ravin des Zouaves-1, we attribute the cranial fragment SNSB-BSPG-1899 VII also to *C. pentelici*.

Subfamily **Amebelodontinae** Barbour, 1927

Genus ***Konobelodon*** Lambert, 1990

Konobelodon atticus (Wagner, 1857)

Material: left mandibular fragment with lower tusk, NHMW-1911-V-49.

Description: The hemimandible is almost complete (preserved length: 310 mm, corpus width: 47 mm, corpus height: 57 mm), missing only a small part from its caudal end with the condyle (Fig. 10a–b). Although the very juvenile stage of the mandible, the symphysis is strong and long (105 mm), and its height (54 mm) is only slightly smaller than that of the corpus. The latter forms an obtuse angle with the ramus. The tip of the lower tusk is broken. It is flattened (width × height: ~23 × 16 mm), bears a thin enamel cap and a weak series of buds is developed on its mesiolateral side. The deciduous dentition is inside the mandibular bone and its morphology is not visible.

Remarks: The presence of a tetralophodont gomphothere in Samos was securely recorded by a cranial and a mandibular specimen with deciduous dentition (Lehmann 1950), which were possibly destroyed during World War II as with the other Samos specimens originally stored at the Munich collections, and therefore a direct comparison is impossible. Based on the descriptions, measurements and the illustration provided by Lehmann (1950: pl. 22, fig. 108), and its comparison with corresponding specimens from Pikermi (AMPG, SNSB-BSPG, MNHN) and Margheh (Iran; NHMW), this material was recently attributed to the tetralophodont amebelodontine *Konobelodon atticus* (Konidaris and Koufos 2013; Konidaris et al. 2014). The mandibular material of *Konobelodon atticus* from Pikermi (type locality), housed at AMPG and MNHN, allows for a comparison of the Samos specimen. Apart from the similar

general morphology of the mandible (Fig. 10), NHMW-1911-V-49 shares with *K. atticus* juvenile mandibles from Pikermi the strong mandibular symphysis with almost equal height as the corpus. The only difference is that in dorsal view of AMPG-PA3936/91 the symphysis is slightly deflected outwards; however, it is straight in other Pikermi mandibles, e.g., MNHN-PIK-1704b (Fig. 10; Konidaris et al. 2014: fig. 3f). Moreover, the presence of a flattened lower tusk with thin enamel and buds implies affinities with this species (Konidaris et al. 2014: fig. 4a–j). The morphology of the Samos mandible and the presence of a flattened lower tusk are clearly different from the other proboscideans from Samos (*Deinotherium*, *Mammut*, *Choerolophodon*), and indicate apparent similarities with *K. atticus* from Pikermi. Therefore, although the deciduous dentition is not visible, the allocation to this taxon is quite confident, taking also into account the features of the lost skull and its dentition (Lehmann 1950; Konidaris et al. 2014).

Biostratigraphic remarks

Most of the so far studied Samos proboscidean specimens belong to old collections and thus lack precise stratigraphic information. However, based on the new excavations and biostratigraphic studies, as well as on the relocation of the old localities and the re-examination of the old mammal collections (Koufos and Nagel 2009), there are some evidences about the biostratigraphic distribution of the Samos proboscideans.

The specimens of *D. proavum* and "*C. pentelici* advanced" specimens, stored at MGL, are labeled as originating from "Andriano" (Fig. 1; Forsyth-Major 1894). The Adrianos ravine is the main fossiliferous area of Samos, stratigraphically located in the upper part of the Mytilinii Formation (Fm), including several fossiliferous spots (Kostopoulos et al. 2009). The previously described "*C. pentelici* advanced" from Mytilinii-1B (MTLB) and the zygodont proboscidean *Mammut* sp. from Mytilinii-1A (MTLA) originated also from the same

stratigraphic horizon (Konidaris and Koufos 2009, 2013). This fossil level represents the Dominant Mammal Assemblage of Samos, which is correlated to the middle Turolian (MN 12), with an estimated age ~7.1 Ma (Koufos et al. 2009).

The majority of the *Choerolophodon pentelici* specimens from Samos belong to its advanced morph (collections HNHM, MGL, NHMA, NHMW, SMF). The specimens HLMD-SS 230 and the lost SNSB-BSPG-1899 VII of Lehmann (1950) are the only evidences for the presence of "*C. pentelici* primitive" in Samos. According to Konidaris et al. (2016) and Konidaris and Koufos (2016) "*C. pentelici* primitive" is known from the late Vallesian (Xirochori-1, Ravin de la Pluie, Ravin des Zouaves-1) until the early Turolian (Kocherinovo-2, 3, Kemiklitepe-D). The primitive *C. pentelici* from Samos could potentially originate from the basal part of the Mytilinii Fm. Two localities are known from the lower horizons of Mytilinii Fm, Vryssoula and Qx (Fig. 1) (Kostopoulos et al. 2009; Koufos et al. 2009). Several researchers proposed different chronostratigraphic schemes for the Samos fossiliferous localities (Koufos et al. 2009: tab. 1), but there is a general consensus that Vryssoula and Qx are located in the lower part of the Mytilinii Fm, and are correlated to the early Turolian (MN 11). For this lower part, Kostopoulos et al. (2003) and Koufos et al. (2009) based on bio- and magnetostratigraphy proposed an age between 8.0 and 7.6 Ma. Almost contemporaneous is the geographically close locality Kemiklitepe-D (Turkey), where bio- and magnetostratigraphy indicated an age between ~7.9–7.6 Ma and a correlation to the early Turolian (Bonis et al. 1994; Sen et al. 1994). The fauna of the Kocherinovo localities (Bulgaria) is correlated also to the early Turolian (Hristova et al. 2013). All the above mentioned localities include "*C. pentelici* primitive". However, during the early Turolian in continental Greece "*C. pentelici* advanced" is present in Nikiti-2 and Ravin des Zouaves-5 (Konidaris et al. 2016), dated at 8.7–8.2 Ma (biochronology) and ~8.2 Ma (magnetostratigraphy, biochronology), respectively (Koufos et al. 2016). Therefore, either we have to assume that some of the datings are not totally secure or the two morphs co-existed during the early Turolian in different geographic regions. In

conclusion, although the exact dating of the final replacement of the primitive by the advanced *C. pentelici* is not clear yet, this event occurred during the early Turolian, because the advanced morph is certainly known from the middle Turolian (MN 12) in Pikermi [old collections dated at ~7.3 Ma (Böhme et al. 2017)] and the upper part of the main fossiliferous beds in Samos at ~7.1 Ma (Kostopoulos et al. 2003; Koufos et al. 2009) and continues until the late Turolian (MN 13) localities of Dytiko in Axios Valley (Greece; Konidaris, 2013).

Conclusions

Proboscideans are relatively rare in most of the Miocene fossiliferous localities, and therefore any new and especially well-preserved or more complete specimen may add important morphological and biostratigraphic information, and contribute to the better knowledge of this mammal group. Indeed, the deinothere cranium and mandible SMF-M 3604 represent not only the most complete juvenile skull of *Deinotherium proavum*, but to our knowledge of all known Miocene juvenile deinotheres of Eurasia and Africa. The MGL material from "Andriano" indicates the presence of *D. proavum* and of the advanced morph of *Choerolophodon pentelici* in Samos at ~7.1 Ma, together with the previously described zygodont *Mammut* sp. Moreover, the presence of a *C. pentelici* specimen (HLMD-SS 230) with more primitive features marks the first record of "*C. pentelici* primitive" in Samos and further confirms the presence of this morph in the early Turolian of the wider region. Finally, the presence of the tetralophodont amebelodontine *Konobelodon atticus* was already reported during the last years, but based on a material that is not available for direct study. The juvenile mandible NHMW-1911-V-49 validates the presence of this shovel-tusker in the Samos proboscidean assemblage. The presence of *Deinotherium proavum*, *Mammut* sp., *Choerolophodon pentelici* and *Konobelodon atticus*, is typical of the Turolian proboscidean fauna of Southeastern Europe.

Acknowledgments

We would like to thank O. Sandrock (HLMD), R. Marchant (MGL), U. Göhlich (NHMW) and R. Brocke (SMF) for allowing us access to the Samos collections, and W. von Koenigswald (Universität Bonn) for directing our attention to the SMF deinothere. We thank also U. Kotthof (GPIH), L. Kordos (HGI), S. Sen and P. Tassy (MNHN), and G. Rössner (SNSB-BSPG) for granting us access to collections at their disposal. G.E.K. was supported by the European Union-funded Integrated Activities grant SYNTHESYS (AT-TAF-3825, HU-TAF-1683) and by the ERC CoG no. 724703 (CROSSROADS). We thank the reviewers U. Göhlich and M. Gasparik for making constructive comments and suggestions.

References

Aiglstorfer, M., U.B. Göhlich, M. Böhme, and M. Gross. 2014. A partial skeleton of *Deinotherium* (Proboscidea, Mammalia) from the late Middle Miocene Gratkorn locality (Austria). *Palaeobiodiversity and Palaeoenvironments* 94: 49–70.

Bakalov, P., and I. Nikolov. 1962. *Les fossiles de Bulgarie. X. Mammifères tertiaires*. Sofia: Académie des Sciences de Bulgarie.

Bakalow, P. 1914. Beiträge zur Paläontologie Bulgariens. II. Dinotheriumreste aus Bulgarien. *Annuaire de l'Université de Sofia* 8–9: 1–29.

Barbour, E.H. 1927. Preliminary notice of a new proboscidean *Amebelodon fricki*, gen. et sp. nov. *Bulletin of the Nebraska State Museum* 13: 131–134.

Böhme, M., N. Spassov, M. Ebner, D. Geraads, L. Hristova, U. Kirscher, S. Kötter, U. Linnemann, J. Prieto, S. Roussiakis, G. Theodorou, G. Uhlig, and M. Winklofer. 2017. Messinian age and savannah environment of the possible hominin *Graecopithecus* from Europe. *PLoS ONE* 12: e0177347.

Bonaparte, C.L. 1845. *Catalogo Metodico dei Mammiferi Europei*. Milan: Coi tipi di Luigi di Giacomo Pirola.

Bonis, L. de, G. Bouvrain, D. Geraads, G.D. Koufos, S. Sen, and P. Tassy. 1994. Les gisements de mammifères du Miocène supérieur de Kemiklitepe, Turquie: 11. Biochronologie, paléoécologie et relations paléobiogéographiques. *Bulletin du Muséum National d'Histoire Naturelle* 16: 225–240.

Daxner-Höck, G., and U.B. Göhlich. 2009. The early Vallesian vertebrates of Atzelsdorf (Late Miocene, Austria) 1. Introduction. *Annalen des Naturhistorischen Museums in Wien, Serie A* 111: 475–478.

Drevermann, F. 1930. Aus der Zeit des dreizehigen Pferdes. *Natur und Museum* 60: 2–13.

Duranthon, F., P.O. Antoine, D. Laffont, and M. Bilotte. 2007. Contemporanéité de *Prodeinotherium* et *Deinotherium* (Mammalia, Proboscidea) à Castelnau-Magnoac (Hautes-Pyrénées, France). *Revue de Paléobiologie* 26: 403–411.

Eichwald, E. 1831. *Zoologia specialis quam expositis animalibus tum vivis, tum fossilibus potissimum Rossiae in universum, et Poloniae in specie*. Vilnae: Josephi Zawadzki.

Forsyth Major, C.J. 1888. Sur un gisement d'ossements fossiles dans l' île de Samos, contemporains de l' âge de Pikermi. *Comptes Rendus Hebdomadaires des Séances de l'Académie des Sciences* 107: 1178–1181.

Forsyth Major, C.J. 1894. *Le gisement ossifère de Mytilinii et catalogue d'ossements fossiles recueillis à Mitylini, île de Samos, et déposés au Collège Galliard à Lausanne*. Lausanne: Georges Bridel & Cie.

Garevski, R., and G.N. Markov. 2011. A *Deinotherium gigantissimum* (Mammalia, Proboscidea) palate with deciduous dentition from the area of Veles, Republic of Macedonia. *Paläontologische Zeitschrift* 85: 33–36.

Gaudry, A., and E. Lartet. 1856. Résultats des recherches paléontologiques entreprises dans l'Attique sous les auspices de l'Académie. *Comptes Rendus de l'Académie des Sciences de Paris* 43: 271–274.

Gaziry, A.W. 1976. Jungtertiäre Mastodonten aus Anatolien (Türkei). *Geologisches Jahrbuch* 22: 3–143.

Ginsburg, L., and F. Chevrier. 2001. Les Dinothères du bassin de la Loire et l'évolution du genre *Deinotherium* en France. *Symbioses* 5: 9–24.

Göhlich, U.B., and K. Huttunen. 2009. The early Vallesian vertebrates of Atzelsdorf (Late Miocene, Austria) 12. Proboscidea. *Annalen des Naturhistorischen Museums in Wien, Serie A* 111: 635–646.

Gray, J.E. 1821. On the natural arrangements of vertebrose animals. *London Medical Repository* 15: 296–310.

Harris, J.M. 1987. Fossil Deinotheriidae from Laetoli. In *Laetoli: A Pliocene site in northern Tanzania*, eds. M.D. Leakey, and J.M. Harris, 294–297. Oxford: Clarendon Press.

Hay, O.P. 1922. Further observations on some extinct elephants. *Proceedings of The Biological Society of Washington* 35: 97–101.

Heizmann, E.P.J., F. Duranthon, and P. Tassy. 1996. Miozäne Großsäugetiere. *Stuttgarter Beiträge zur Naturkunde, Serie C* 39: 1–60.

Hristova, L., D. Geraads, G.N. Markov, and N. Spassov. 2013. Late Miocene mammals from Kocherinovo, Southwestern Bulgaria. *Acta zoologica bulgarica* 65: 517–529.

Huttunen, K., 2002. Systematics and Taxonomy of the European Deinotheriidae (Proboscidea, Mammalia). *Annalen des Naturhistorischen Museums in Wien, Serie A* 103: 237–250.

Illiger, C. 1811. *Prodromus systematis mammalium et avium additis terminis zoographicis utriusque classis*. Berlin: C. Salfield.

Jourdan, M. 1861. Des terrains sidérolitiques. *Comptes Rendus Hebdomadaires des Séances de l'Académie des Sciences* 53: 1009–1014.

Kaup, J. J. 1829. Neues Säugthier, *Deinotherium*: *Deinotherium giganteum*. *Isis* 22: 401–404.

Kaup, J.J. 1832. *Description d'ossements fossiles de mammifères inconnus jusqu'à présent, qui se trouvent au Muséum grand-ducal de Darmstadt*. Darmstadt: J.G. Heyer.

Khomenko, J. 1914. La faune méotique du village Taraklia du district de Bendery. *Trudy Bessarabskago Obshestva Estestvoispytatelei i liubitelei estestvoznania* 5: 1–55.

Konidaris, G.E. 2013. *Palaeontological and biostratigraphical study of the Neogene Proboscidea from Greece*. Ph.D. thesis. Thessaloniki: Aristotle University of Thessaloniki.

Konidaris, G.E., and G.D. Koufos. 2009. The Late Miocene Mammal Faunas of the Mytilinii Basin, Samos Island, Greece: New Collection. 8. Proboscidea. In *The Late Miocene Mammal Faunas of Samos*, eds. G.D. Koufos, and D. Nagel. *Beiträge zur Paläontologie* 31: 139–155.

Konidaris, G.E, and G.D Koufos. 2013. Late Miocene Proboscidea (Mammalia) from Macedonia and Samos Island, Greece: preliminary results. *Paläontologische Zeitschrift* 87: 121–140.

Konidaris, G.E., and G.D. Koufos. 2016. Proboscidea. In *Palaeontology of the upper Miocene vertebrate localities of Nikiti (Chalkidiki Peninsula, Macedonia, Greece)*, eds. G.D. Koufos, and D.S. Kostopoulos. *Geobios* 49: 37–44.

Konidaris, G.E., S.J. Roussiakis, G.E. Theodorou, and G.D. Koufos. 2014. The Eurasian occurrence of the shovel-tusker *Konobelodon* (Mammalia, Proboscidea) as illuminated by its presence in the late Miocene of Pikermi (Greece). *Journal of Vertebrate Paleontology* 34: 1437–1453.

Konidaris, G.E., G.D. Koufos, D.S. Kostopoulos, and G. Merceron. 2016. Taxonomy, biostratigraphy and palaeoecology of *Choerolophodon* (Proboscidea, Mammalia) in the Miocene of SE Europe-SW Asia: implications for phylogeny and biogeography. *Journal of Systematic Palaeontology* 14: 1–27.

Konidaris, G.E., S.J. Roussiakis, A. Athanassiou, and G.E. Theodorou. 2017. The huge-sized deinothere *Deinotherium proavum* (Proboscidea, Mammalia) from the Late Miocene localities Pikermi and Halmyropotamos (Greece). *Quaternary International* 430: 5–21.

Kostopoulos, D.S., S. Sen, and G.D. Koufos. 2003. Magnetostratigraphy and revised chronology of the late Miocene mammal localities of Samos, Greece. *International Journal of Earth Sciences* 92: 779–794.

Kostopoulos, D.S, G.D. Koufos, I.A. Sylvestrou, G.E. Syrides, and E. Tsombachidou. 2009. The Late Miocene Mammal Faunas of the Mytilinii Basin, Samos Island, Greece: New Collection. 2. Lithostratigraphy and fossiliferous sites. In *The Late Miocene mammal faunas of Samos*, eds. G.D. Koufos, and D. Nagel. *Beiträge zur Paläontologie* 31: 13–26.

Koufos, G.D., and D. Nagel, eds. 2009. *The Late Miocene mammal faunas of Samos*. Vienna: Beiträge zur Paläontologie 31.

Koufos, G.D., D.S Kostopoulos, and T.D. Vlachou. 2009. The Late Miocene Mammal Faunas of the Mytilinii Basin, Samos Island, Greece: New Collection. 16. Biochronology. In *The Late Miocene mammal faunas of Samos*, eds. G.D. Koufos, and D. Nagel. *Beiträge zur Paläontologie* 31: 397–408.

Koufos, G.D., D.S. Kostopoulos, T.D. Vlachou, and G.E. Konidaris. 2016. Synthesis. In *Palaeontology of the upper Miocene vertebrate localities of Nikiti (Chalkidiki Peninsula, Macedonia, Greece)*, eds. G.D. Koufos, and D.S. Kostopoulos. *Geobios* 49: 147–154.

Lambert, W.D. 1990. Rediagnosis of the genus *Amebelodon* (Mammalia, Proboscidea, Gomphotheriidae), with a new subgenus and species, *Amebelodon* (*Konobelodon*) *britti*. *Journal of Paleontology* 64: 1032–1040.

Lartet, E. 1859. Sur la dentition des proboscidiens fossiles (*Dinotherium*, Mastodontes et Éléphants) et sur la distrubution géographique et stratigraphique de leurs débris en Europe. *Bulletin de la Société géologique de France* 16: 469–515.

Lehmann, U. 1950. Über Mastodontenreste in der Bayerischen Staatssammlung in München. *Palaeontographica Abt. A* 99: 121–228.

Linnaeus, C. 1758. *Systema naturae per regna tria naturae, secundum classes, ordines, genera, species, cum characteribus, differentiis, synonymis locis. Tomus 1*. Stockholm: Laurentius Salvius.

Markov, G.N. 2004. The fossil proboscideans of Bulgaria and the importance of some Bulgarian finds - a brief review. *Historia naturalis bulgarica* 16: 139–150.

Markov, G.N. 2008. The Turolian proboscideans (Mammalia) of Europe: preliminary observations. *Historia naturalis bulgarica* 19: 153–178.

Meyer, H. von. 1831. Mittheilung an geheimen Rath von Leonhard. *Jahrbuch für Mineralogie* 1831: 296–297.

Osborn, H.F. 1921. The evolution, phylogeny, and classification of the Proboscidea. *American Museum Novitates* 1: 1–15.

Ozansoy, F. 1965. Étude des gisements continentaux et des mammifères du Cénozoïque de Turquie. *Mémoires de la Société Géologique de France* 102: 1–92.

Pickford, M., and Z. Pourabrishami. 2013. Deciphering Dinotheriensande deinotheriid diversity. *Palaeobiodiversity and Palaeoenvironments* 93: 121–150.

Sach, V.J., and E.P.J. Heizmann. 2001. Stratigraphie und Säugetierfaunen der Brackwassermolasse in der Umgebung von Ulm (Südwestdeutschland). *Stuttgarter Beiträge zur Naturkunde, Serie B* 310: 1–95.

Sanders, W.J. 2003. Proboscidea. In *Geology and Paleontology of the Miocene Sinap Formation, Turkey*, eds. M. Fortelius, J. Kappelman, S. Sen, and R.L. Bernor, 202–219. New York: Columbia University Press.

Schlesinger, G. 1917. Die Mastodonten des K. K. Naturhistorischen Hofmuseums. *Denkschriften des K. K. Naturhistorischen Hofmuseums* 1: 1–230.

Schlesinger, G. 1922. Die Mastodonten der Budapester Sammlungen. *Geologica Hungarica* 2: 1–284.

Sen, S., L. de Bonis, N. Dalfes, D. Geraads, and G.D. Koufos. 1994. Les gisements de mammifères du Miocène supérieur de Kemiklitepe, Turquie: 1. Stratigraphie et magnétostratigraphie. *Bulletin du Muséum National d'Histoire Naturelle* 16: 5–17.

Simionescu, I., and V. Barbu. 1939. Mamiferele pliocene dela Cimişlia (România). III. Proboscidieni. *Academia Română Publicaţiunile Fondului V. Adamachi* 9: 1–20.

Solounias, N. 1981. The Turolian fauna from the Island of Samos, Greece. With special emphasis on the hyaenids and the bovids. *Contributions to Vertebrate Evolution* 6: 1–232.

Spassov, N., and G.D. Koufos. 2002. The first appearance of *Dinocrocuta gigantea* and *Machairodus aphanistus* (Mammalia, Carnivora) in the Miocene of Bulgaria. *Mitteilungen der Bayerischen Staatssammlung für Paläontologie und historische Geologie* 42: 83–101.

Stefanescu, G. 1892. On the existence of the *Dinotherium* in Roumania. *Bulletin of the Geological Society of America* 3: 81–83.

Stehlin, H.G. 1925. Catalogue des ossements de mammifères Tertiaires de la collection Bourgeois à l'École de Pont-Levoy (Loir-et-Cher). *Bulletin de la Société d'Histoire naturelle et d'Anthropologie de Loir-et-Cher* 18: 77–277.

Tarabukin, B.A. 1974. New data on the systematics, phylogeny and ecology of Suborder Deinotherioidea Osborn (1921). In *Mammals of the late Cenozoic from Southwestern USSR*, eds. A.I. David, M.N. Lozan, and B.A. Trofimov, 77–90. Izd. Shtiinsta: Kishinev.

Tassy, P. 1994. Les gisements de mammifères du Miocène supérieur de Kemiklitepe, Turquie: 7. Proboscidea (Mammalia). *Bulletin du Muséum National d'Histoire Naturelle* 16: 143–157.

Tassy, P. 1996a. Dental homologies and nomenclature in the Proboscidea. In *The Proboscidea: Evolution and palaeoecology of elephants and their relatives*, eds. J. Shoshani, and P. Tassy, 21–25. New York: Oxford University Press.

Tassy, P. 1996b. Growth and sexual dimorphism among Miocene elephantoids: the example of *Gomphotherium angustidens*. In *The Proboscidea: Evolution and palaeoecology of elephants and their relatives*, eds. J. Shoshani, and P. Tassy, 92–100. New York: Oxford University Press.

Tassy, P. 2005. Proboscideans (Mammalia) from the late Miocene of Akkaşdağı, Turkey. In *Geology, mammals and environments at Akkaşdağı, late Miocene of Central Anatolia*, ed. S. Sen. *Geodiversitas* 27: 707–714.

Wagner, A. 1857. Neue Beiträge zur Kenntnis der fossilen Säugthier-Ueberreste von Pikermi. *Abhandlungen der Bayerischen Akademie der Wissenschaften* 8: 109–158.

FIGURE AND TABLE CAPTIONS

Fig. 1 Geographic position of Samos (www.shadedrelief.com and Google Earth), geological map of the Mytilinii Basin showing the old and new fossiliferous sites (from Kostopoulos et al. 2003 and references cited therein), and stratigraphic column of the Mytilinii Formation with the position of the sites and their age based on bio- and magnetostratigraphy (from Kostopoulos et al. 2003, 2009; Koufos et al. 2009).

Fig. 2 *Deinotherium proavum* from Samos. **a–f,** partial cranium with the DP2–DP4 of both sides (**a–d**) and associated mandible with the dp2–dp4 of both sides (**e–f**), SMF-M 3604; in **a,** left lateral, **b,** dorsal, **c,** ventral, **d,** caudal (damaged), **e,** left lateral, and **f,** dorsal view; **g–h,** right mandibular fragment with partial lower tusk and the dp3–dp4, MGL-S 1048 and MGL-S 380, "Adriano"; in **g,** dorsal, and **h,** right lateral view; **i,** left mandibular fragment with the dp4, MGL-381, "Andriano", dorsal view.

Fig. 3 *Deinotherium proavum* from Samos. **a,** right DP2–DP4, SMF-M 3604, occlusal view; **b,** right dp2–dp4, SMF-M 3604, occlusal view; **c,** dp3–dp4, MGL-S 1048 and MGL-S 380, occlusal view.

Fig. 4 Metrical and morphological comparison of deinothere deciduous teeth from various localities. **a,** biplots comparing the length and width; the symbol "?" indicates incomplete or inadequately preserved specimens; data from Khomenko (1914), Stehlin (1925), Simionescu and Barbu (1939), Gaziry (1976), Ginsburg and Chevrier (2001), Sach and Heizmann (2001), Huttunen (2002), Göhlich and Huttunen (2009), Garevski and Markov (2011), Konidaris et al. (2017) and own measurements at FSL, HGI, HLMD, MGL, ML, SMF, SNSB-BSPG and SU; **b–i,** dp2 morphology of several deinotheres and angle between the ectolophid and the long axis of the tooth; **b,** *P. cuvieri*, Montréal-du-Gers, France, left dp2, GER-620 (from Ginsburg and Chevrier 2001); **c,** *D. levius*, La Grive, France, left dp2, ML-LGR 959; **d,** *D. giganteum*, Montredon, France, right dp2 (reversed), ML-MR-52; **e,** *D. giganteum*, Montredon, France, left dp2, FSL-210393; **f,** *D.* ?*giganteum*, Nessebar, Bulgaria, left dp2, SU-191; **g,** *D.* ?*giganteum*,

Kayadibi, Turkey, left dp2, GPIH-T.K.-Nr. 1822; **h,** *D. proavum*, Pikermi, Greece, left dp2, AMPG-PA3950/91; **i,** *D. proavum*, Samos, Greece, left dp2, SMF-M 3604; **j–o,** DP2 morphology of several deinotheres; **j,** *P. bavaricum*, Tavers, France, right DP2 (reversed), MSNO.D.259 (from Ginsburg and Chevrier 2001); **k,** *P. bavaricum*, Esselborn, Germany, left DP2, HLMD-Din 237; **l,** *D. levius*, La Grive, France, right DP2 (reversed), ML-LGR 970; **m,** *D. levius*, Massenhausen, Germany, right DP2 (reversed), SNSB-BSPG-1959 I 430; **n,** *D. giganteum*, Montredon, France, left DP2, FSL-210255; **o,** *D. proavum*, Samos, Greece, left DP2, SMF-M 3604.

Fig. 5 *Choerolophodon pentelici* from Samos. **a–e,** partial juvenile cranium with the erupting DP4 of both sides (**a–c**) and associated right hemimandible with the dp3 and erupting dp4 (**d–e**), SMF-M 3603; in **a,** anterodorsal, **b,** ventral, **c,** left lateral, **d,** right lateral, **e,** dorsal view.

Fig. 6 *Choerolophodon pentelici* from Samos. **a,** maxilla with right and left DP2–DP3, HLMD-SS 230, ventral view; **b,** right and left mandibular fragments with the dp3s, MGL-S 340, "Andriano", dorsal view; **c,** right dp4 and left mandibular fragment with dp4 and partial m1, MGL-S 333, "Andriano", dorsal view.

Fig. 7 Biplot comparing the length and width of the choerolophodont DP2 MGL-S 614 (right DP2 in occlusal view) from Samos ("Andriano") with choerolophodont DP2s from various localities of Greece, Turkey and Iran. Data from Gaziry (1976), Sanders (2003), Tassy (2005), and own measurements at HGI, LGPUT, MGL, NHMA, NHMW and MNHN.

Fig. 8 Metrical and morphological comparison of the dp3 of *Choerolophodon* from various localities from Greece, Bulgaria, Turkey and Iran. **a,** biplot comparing the length and width; data from Gaziry (1976), Tassy (1994, 2005), Hristova et al. (2013) and own measurements at HGI, LGPUT, MGL, NHMW, MNHN and SMF; **b,** *C. anatolicus*, Yassiören, Turkey, left dp3 (reversed), cast MNHN-YAS-49, early Vallesian; **c,** "*C. pentelici* primitive", Ravin de la Pluie, Greece, left dp3 (reversed), LGPUT-RPl-258, late Vallesian; **d,** "*C. pentelici* advanced", Ravin des Zouaves-5, Greece, left dp3 (reversed), early Turolian; **e,** "*C. pentelici* advanced", Samos,

Greece, right dp3, SMF-M 3603, Turolian; **f,** "*C. pentelici* advanced", Samos ("Andriano"), Greece, left dp3 (reversed), MGL-S 340, middle Turolian; **g,** "*C. pentelici* advanced", Samos, Greece, right dp3, NHMW 2014/0129/0002 (from "Cranium C"), Turolian; **h,** "*C. pentelici* advanced", Pikermi, Greece, right dp3, MNHN-PIK-3665 (from lectotype of *C. pentelici*), middle Turolian.

Fig. 9 Metrical and morphological comparison of the DP3 of *Choerolophodon* from various localities from Greece, Bulgaria, Turkey and Iran. **a,** biplot comparing the length and width; data from Gaziry (1976), Tassy (1994), Sanders (2003), Hristova et al. (2013) and own measurements at HGI, LGPUT, NHMW and MNHN; **b,** *C. anatolicus*, Yassiören, Turkey, right DP3, MNHN-TRQ-1000 (from lectotype of *C. anatolicus*), early Vallesian; **c,** "*C. pentelici* primitive", Xirochori-1, Greece, left DP3 (reversed), LGPUT-XIR-11, late Vallesian; **d,** "*C. pentelici* primitive", Xirochori-1, Greece, right DP3, LGPUT-XIR-12, late Vallesian; **e,** "*C. pentelici* primitive", Samos, Greece, right DP3, HLMD-SS 230, Turolian; **f,** "*C. pentelici* advanced", Nikiti-2, Greece, left DP3 (reversed), LGPUT-NIK-1613, early Turolian; **g,** "*C. pentelici* advanced", Ravin des Zouaves-5, Greece, left DP3 (reversed), LGPUT-RZO-13, early Turolian; **h,** "*C. pentelici* advanced", Pikermi, Greece, left DP3 (reversed), MNHN-PIK-1705, middle Turolian; **i,** "*C. pentelici* advanced", Samos, Greece, left DP3 (reversed), NHMW-2014/0129/0001 ("Cranium B"), Turolian.

Fig. 10 Comparison of the juvenile mandibles of *Konobelodon atticus* from Samos and Pikermi (Greece). **a–b,** left mandibular fragment with lower tusk, NHMW-1911-V-49, Samos; in **a,** left lateral, and **b,** dorsal view; **c,** right mandibular fragment with dp2–dp3, MNHN-PIK-1704b, Pikermi, dorsal view (vertically mirrored); **d–e,** right mandibular fragment with lower tusk and dp2–dp3 in alveolus, AMPG-PA3936/91, Pikermi; in **d,** right lateral (horizontally mirrored), and **e,** dorsal (vertically mirrored) view.

Table 1 Cranial measurements (in mm) of *Deinotherium proavum* and *Choerolophodon pentelici* from Samos (SMF). Measurements according to Tassy (1996b).

Table 2 Mandibular measurements (in mm) of *Deinotherium proavum* and *Choerolophodon pentelici* from Samos (SMF). Measurements according to Tassy (1996b).

Table 3 Dental measurements (in mm) of *Deinotherium proavum* and *Choerolophodon pentelici* from Samos (HLMD, MGL, SMF).

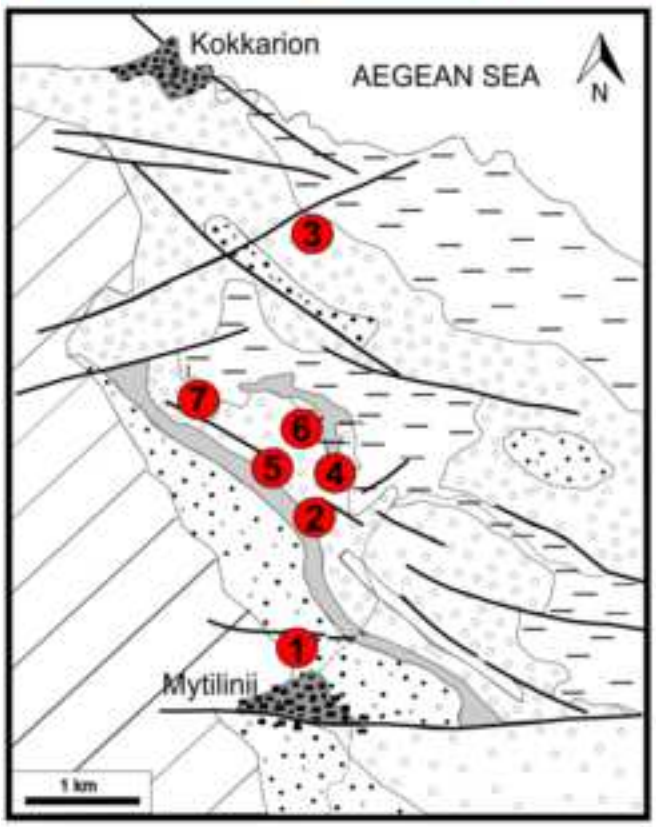

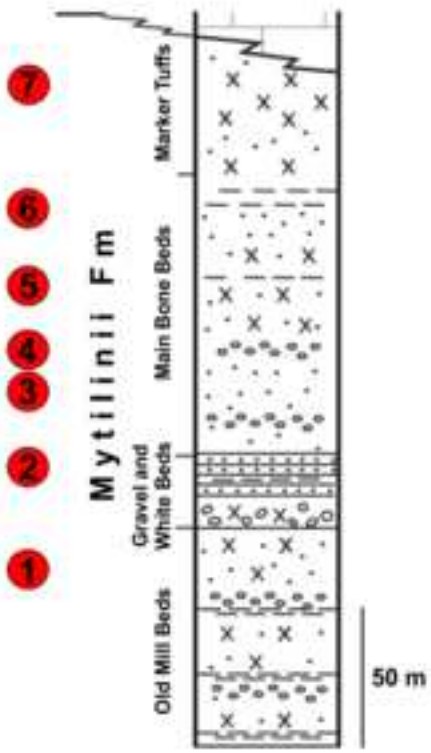

HORA Fm
thick to thin-laminated lacustrine limestones with intercalations of thin beds of tuffaceous clays

MYTILINII Fm

green-brown silty sands,alternating with sandy tuffs, gritstones and conglomerates

white marls and marly-sandy limestones with white limestone breccia and conglomerates

brownish to reddish silty sands with intercalation of tuffs

KOKKARION Fm
Alternating yellowish-white lacustrine limestones, green-brown clays and tuffaceous sands

Alluvial deposits

Fault

1. Vryssoula, Qx → 8.0–7.6 Ma
2. Mytilinii-4 (MLN), Q2, Stefano → ~7.5 Ma
3. Mytilinii-5 (MTN), ?Q6
4. Mytilinii-3 (MYT), Q3, ?Potamies → ~7.3 Ma
5. ?Q4
6. Mytilinii-1 (MTL, A–D), Q1, "Andriano" → ~7.1 Ma
7. Q5 → 6.9–6.7 Ma

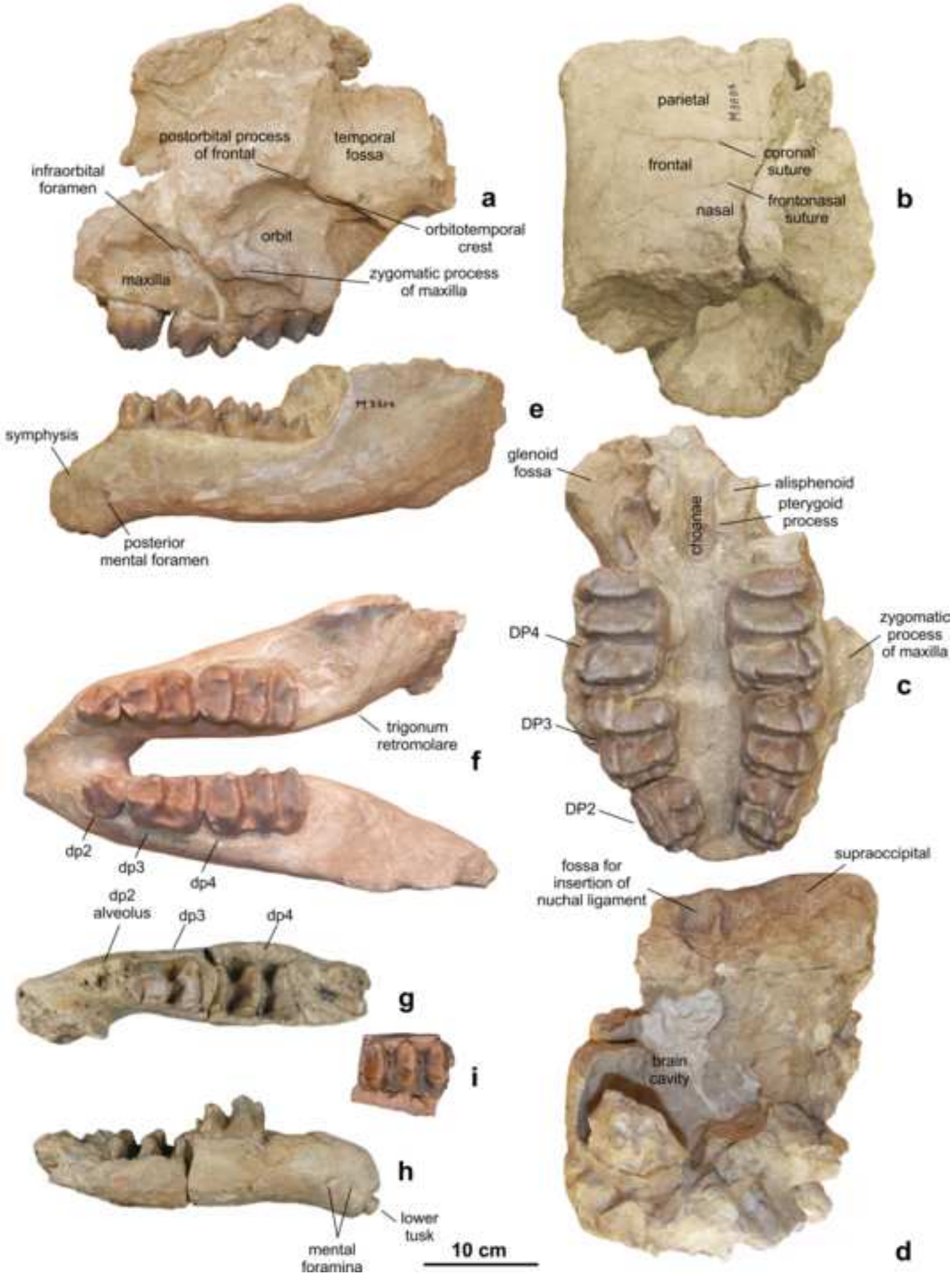
postorbital process of frontal
temporal fossa
infraorbital foramen
orbit
orbitotemporal crest
maxilla
zygomatic process of maxilla
a
parietal
coronal suture
frontal
nasal
frontonasal suture
b
symphysis
posterior mental foramen
e
glenoid fossa
alisphenoid
pterygoid process
choanae
DP4
DP3
DP2
zygomatic process of maxilla
c
trigonum retromolare
f
dp2
dp3
dp4
dp2 alveolus
dp3
dp4
g
i
h
lower tusk
mental foramina
10 cm
fossa for insertion of nuchal ligament
supraoccipital
brain cavity
d

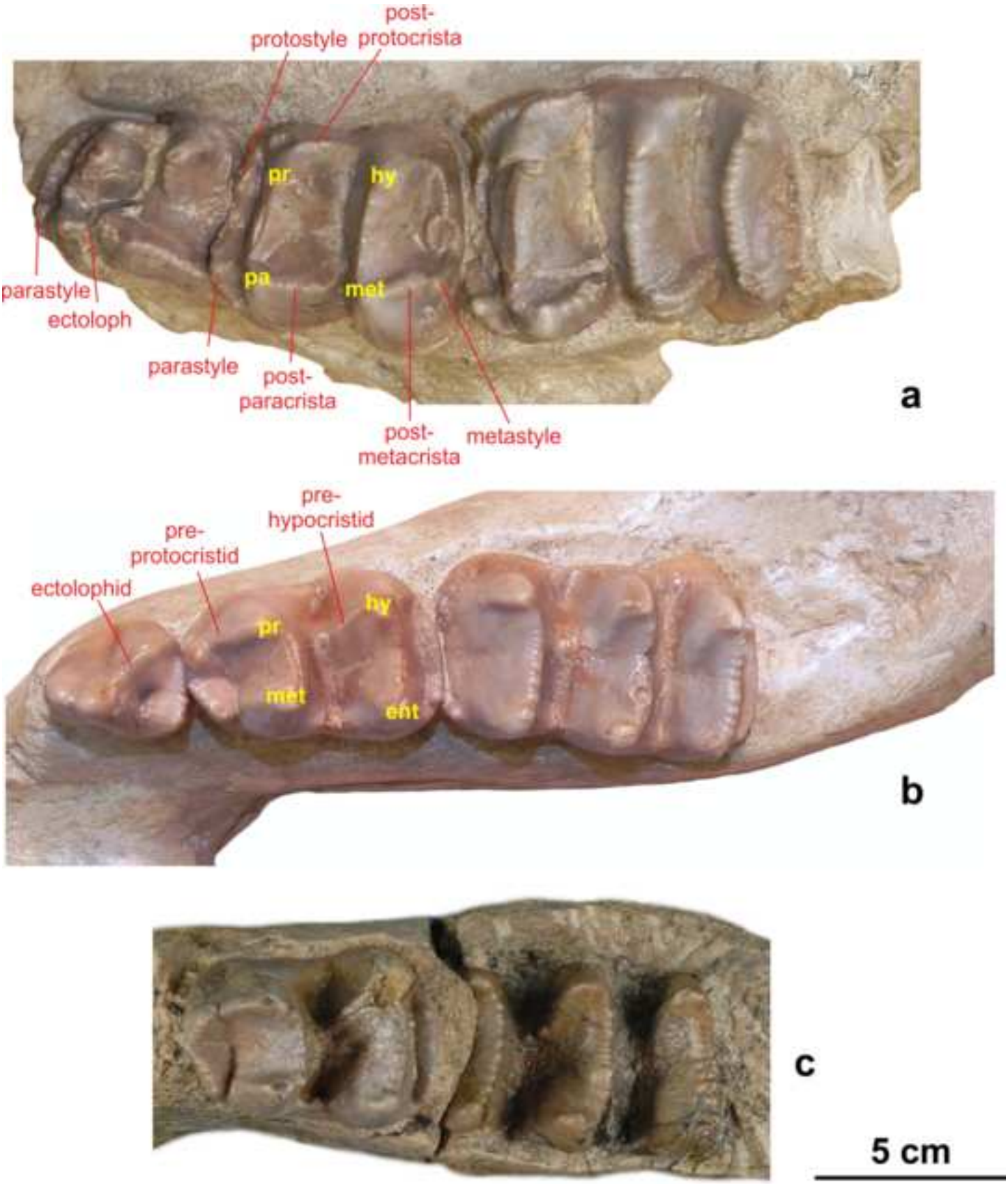
post-
protocrista
protostyle
pr
hy
pa
met
parastyle
ectoloph
parastyle
post-
paracrista
post-
metacrista
metastyle
a
pre-
hypocristid
pre-
protocristid
ectolophid
hy
pr
met
ent
b
c
5 cm

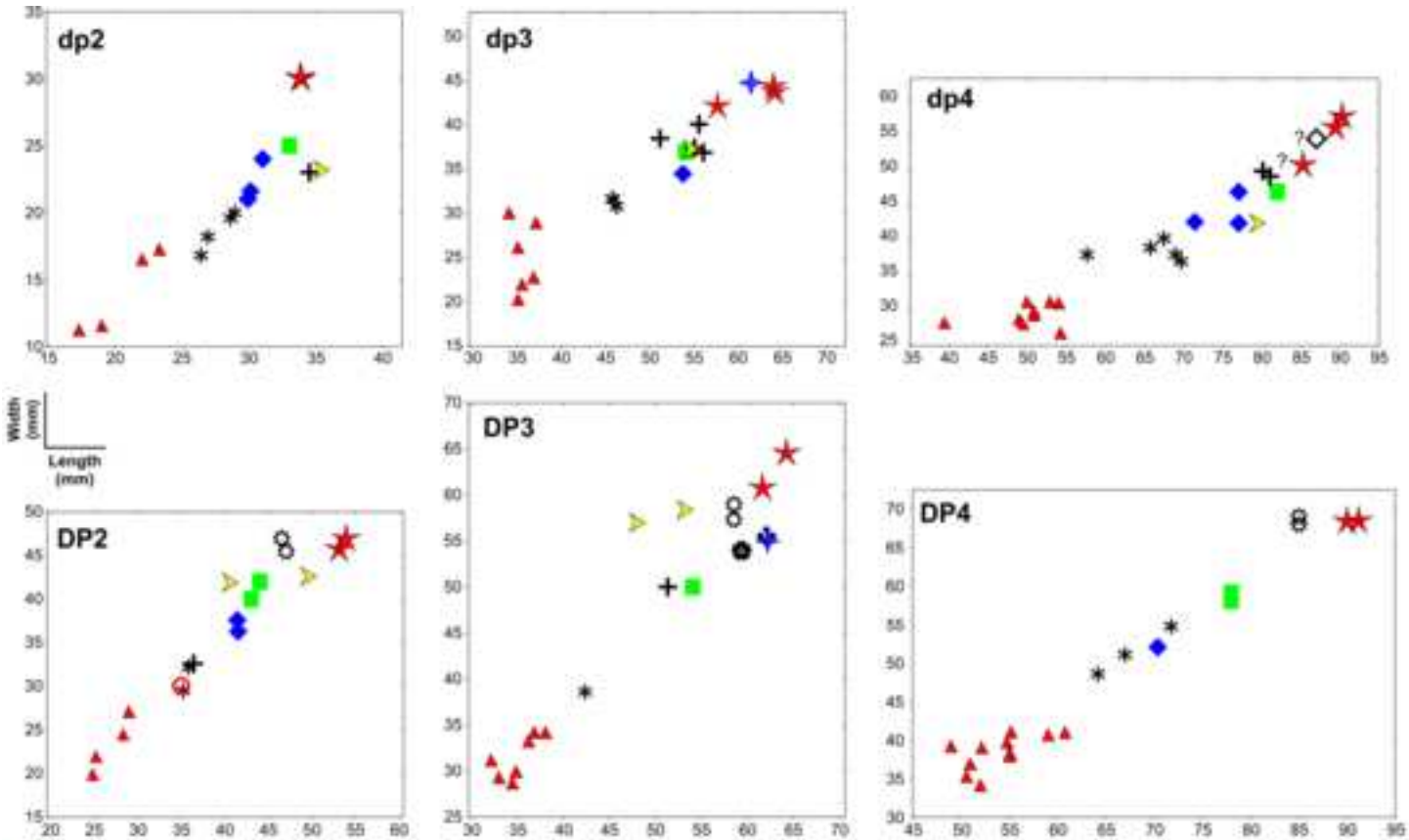

▲ *Prodeinotherium*, MN 4–MN 6
[*P. cuvieri* and *P. bavaricum* from several localities in France (Stehlin 1925; Ginsburg and Chevrier 2001) and Langenau 1, Germany (Sach and Heizmann 2001)]

✱ *Deinotherium levius*, MN 7/8
[La Grive, France (ML) and Massenhausen, Germany (SNSB-BSPG)]

○ *Deinotherium ?levius*, Atzelsdorf, Austria, early MN 9 (Göhlich and Huttunen 2009)

◆ *D. giganteum*, Montredon, France, MN 10 (FSL, ML)

■ *D. ?giganteum*, Kayadibi, Turkey, late Miocene (Gaziry 1976)

✚ *D. ?giganteum*, Nessebar, Bulgaria, late Miocene (SU)

D. proavum

➤ Pikermi, Greece, MN 12 (Konidaris et al. 2017)

✣ Cimislia, Moldova, MN 12 (Khomenko 1914)

⬢ Taraklia, Moldova, MN 12 (Simionescu and Barbu 1939)

✦ Baltavár, Hungary, MN 12 (HGI)

◇ Polgárdi, Hungary, MN 13 (HGI)

⬡ Kiro Kucuk, FYROM, Turolian (Garevski and Markov 2011)

★ Samos, Greece, Turolian (MGL, SMF)

a

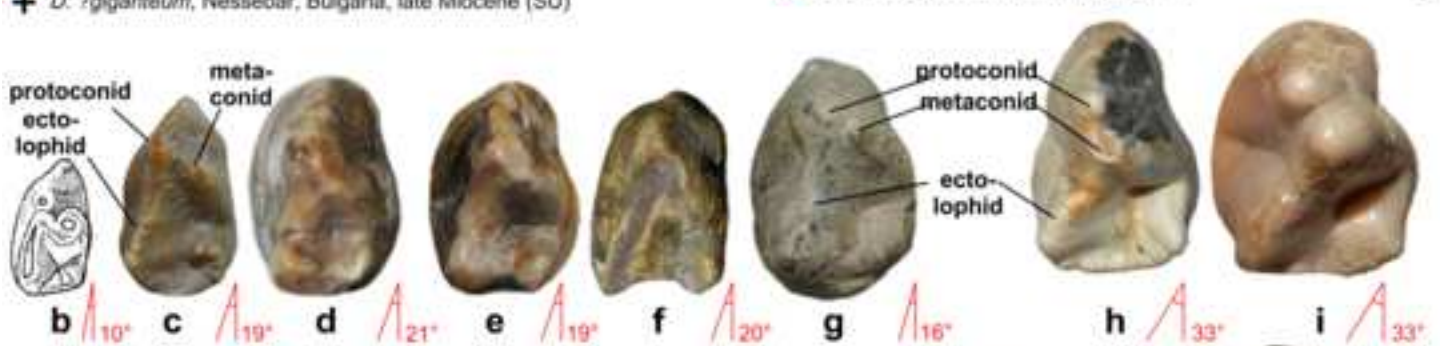

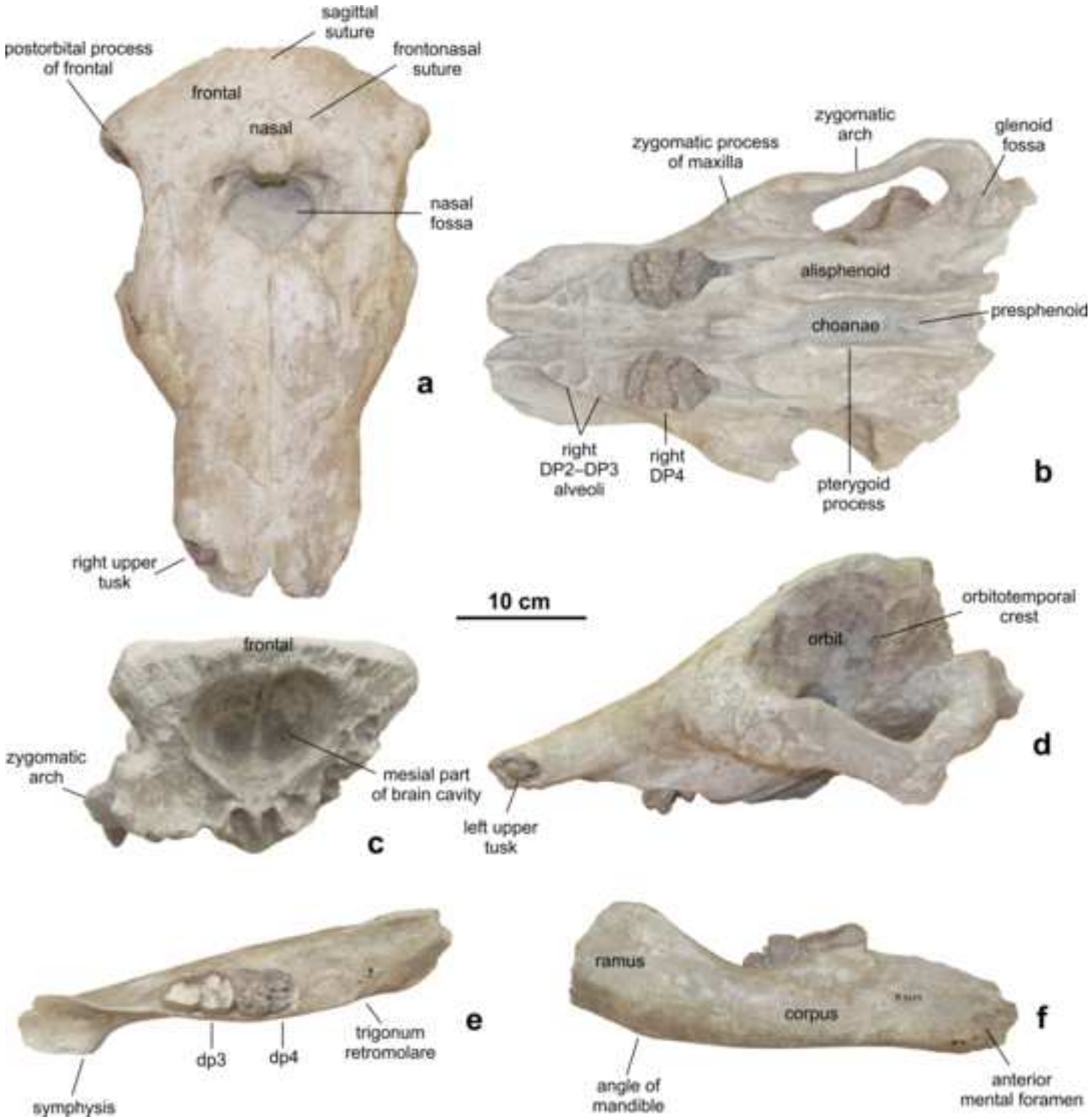
sagittal suture
postorbital process of frontal
frontonasal suture
frontal
nasal
nasal fossa
a
right upper tusk
zygomatic arch
glenoid fossa
zygomatic process of maxilla
alisphenoid
presphenoid
choanae
right DP2–DP3 alveoli
right DP4
pterygoid process
b
10 cm
orbitotemporal crest
orbit
d
left upper tusk
frontal
zygomatic arch
mesial part of brain cavity
c
trigonium retromolare
dp3
dp4
symphysis
e
ramus
corpus
f
angle of mandible
anterior mental foramen

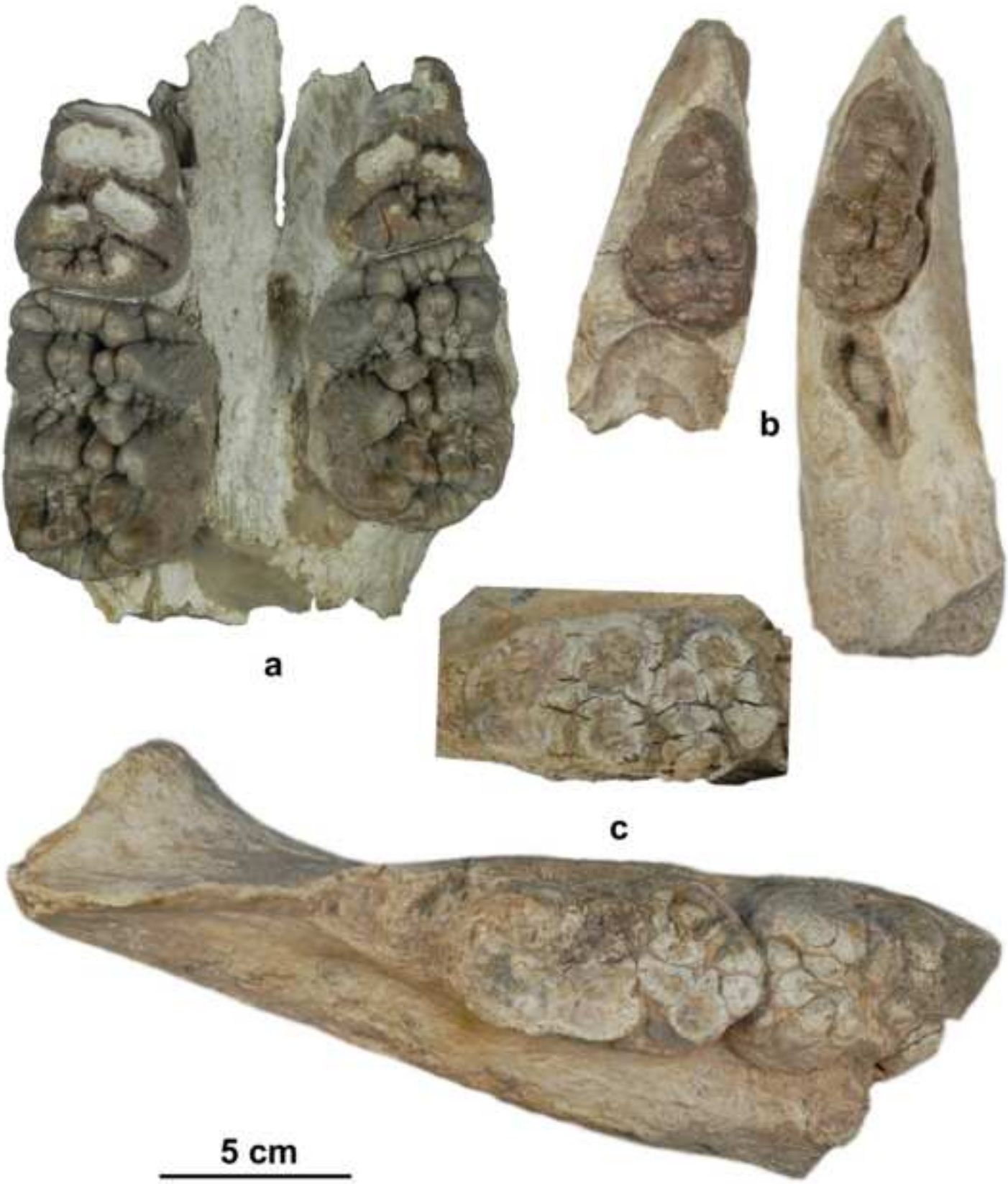
a
b
c
5 cm

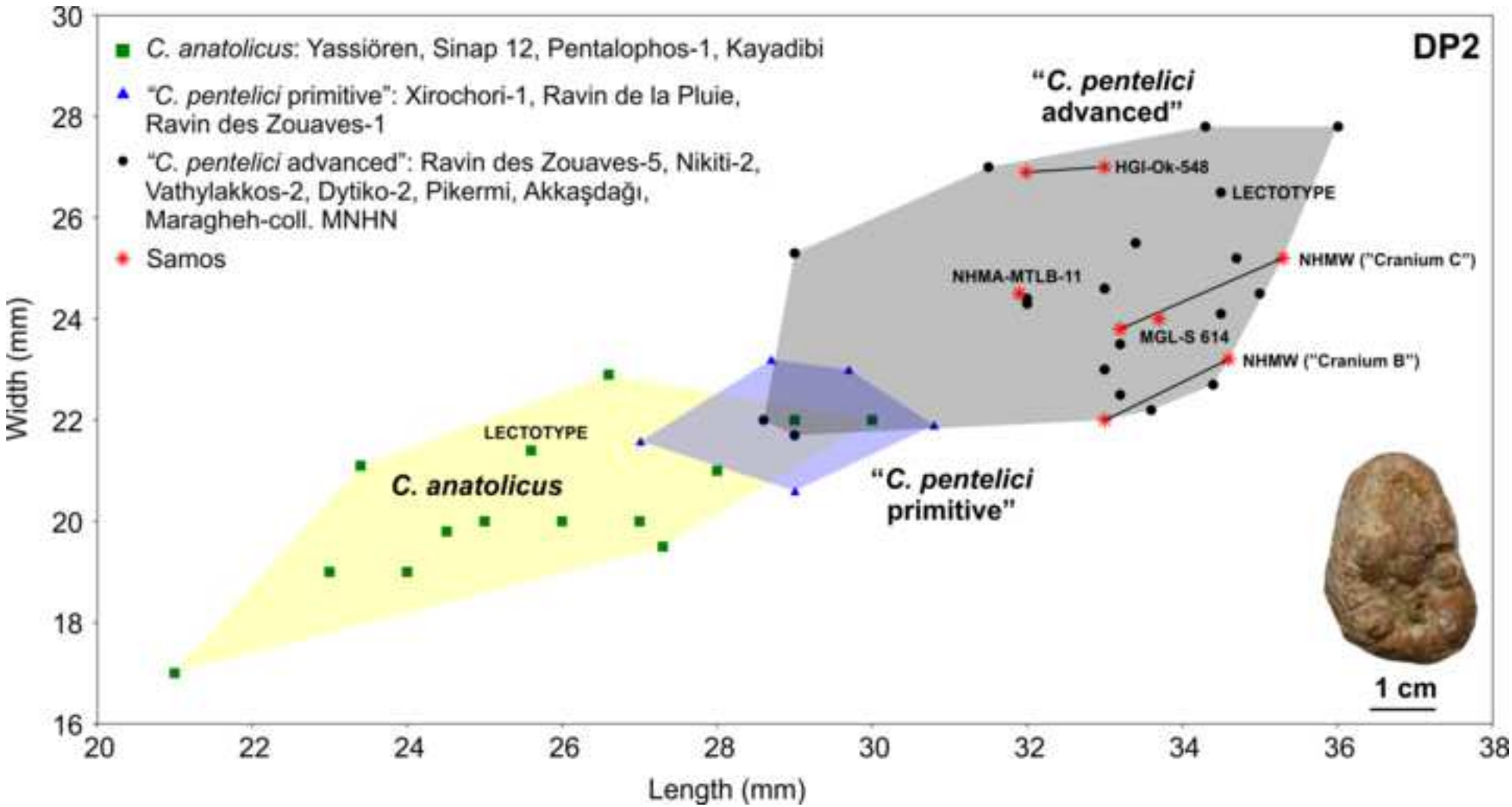
DP2
C. anatolicus: Yassiören, Sinap 12, Pentalophos-1, Kayadibi
"C. pentelici primitive": Xirochori-1, Ravin de la Pluie, Ravin des Zouaves-1
"C. pentelici advanced": Ravin des Zouaves-5, Nikiti-2, Vathylakkos-2, Dytiko-2, Pikermi, Akkaşdağı, Maragheh-coll. MNHN
Samos
"C. pentelici advanced"
HGI-Ok-548
LECTOTYPE
NHMW ("Cranium C")
NHMA-MTLB-11
MGL-S 614
NHMW ("Cranium B")
LECTOTYPE
C. anatolicus
"C. pentelici primitive"
1 cm
Width (mm)
Length (mm)
16
18
20
22
24
26
28
30
20
22
24
26
28
30
32
34
36
38

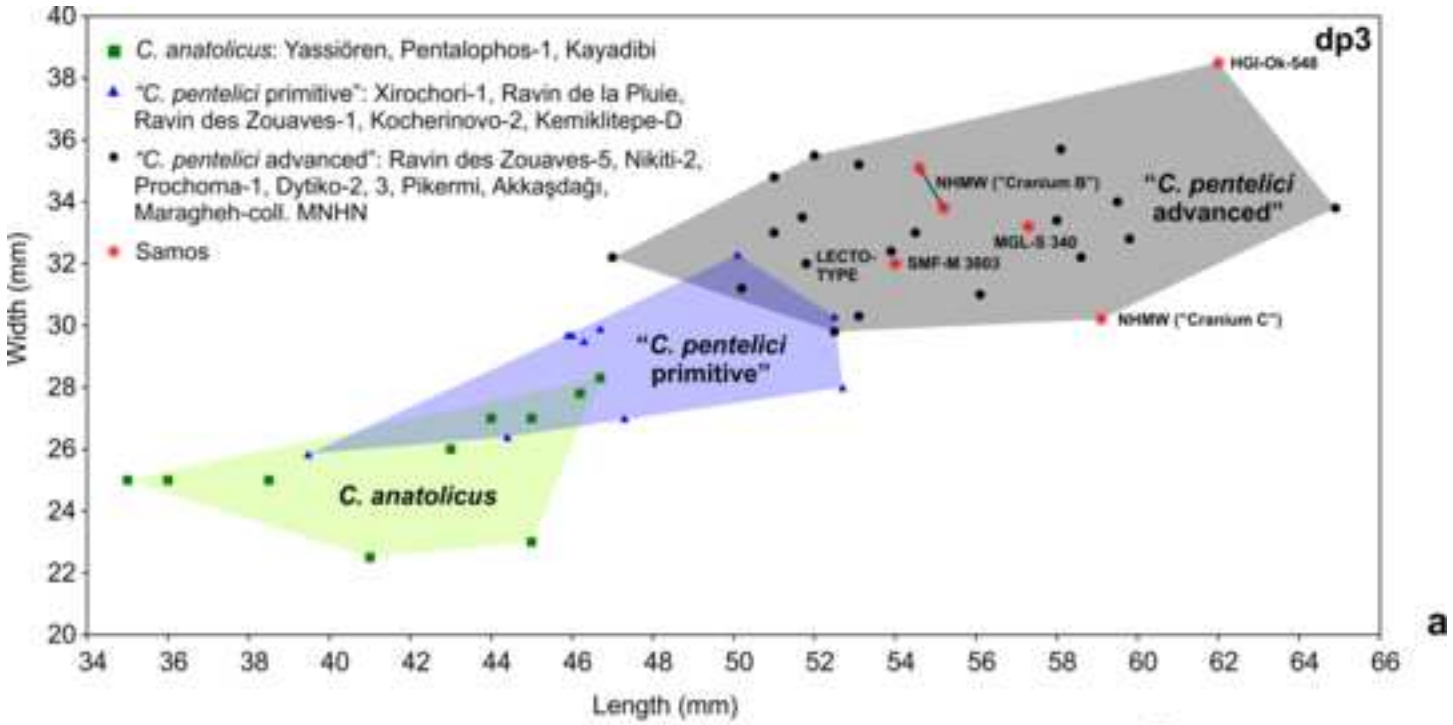
dp3
C. anatolicus: Yassiören, Pentalophos-1, Kayadibi
"C. pentelici primitive": Xirochori-1, Ravin de la Pluie, Ravin des Zouaves-1, Kocherinovo-2, Kemiklitepe-D
"C. pentelici advanced": Ravin des Zouaves-5, Nikiti-2, Prochoma-1, Dytiko-2, 3, Pikermi, Akkaşdağı, Maragheh-coll. MNHN
Samos
"C. pentelici advanced"
"C. pentelici primitive"
C. anatolicus
HGI-Ok-548
NHMW ("Cranium B")
MGL-S 340
LECTO-TYPE
SMF-M 3803
NHMW ("Cranium C")
Width (mm)
Length (mm)
a


b
c
d
e

1 cm


f
g
h

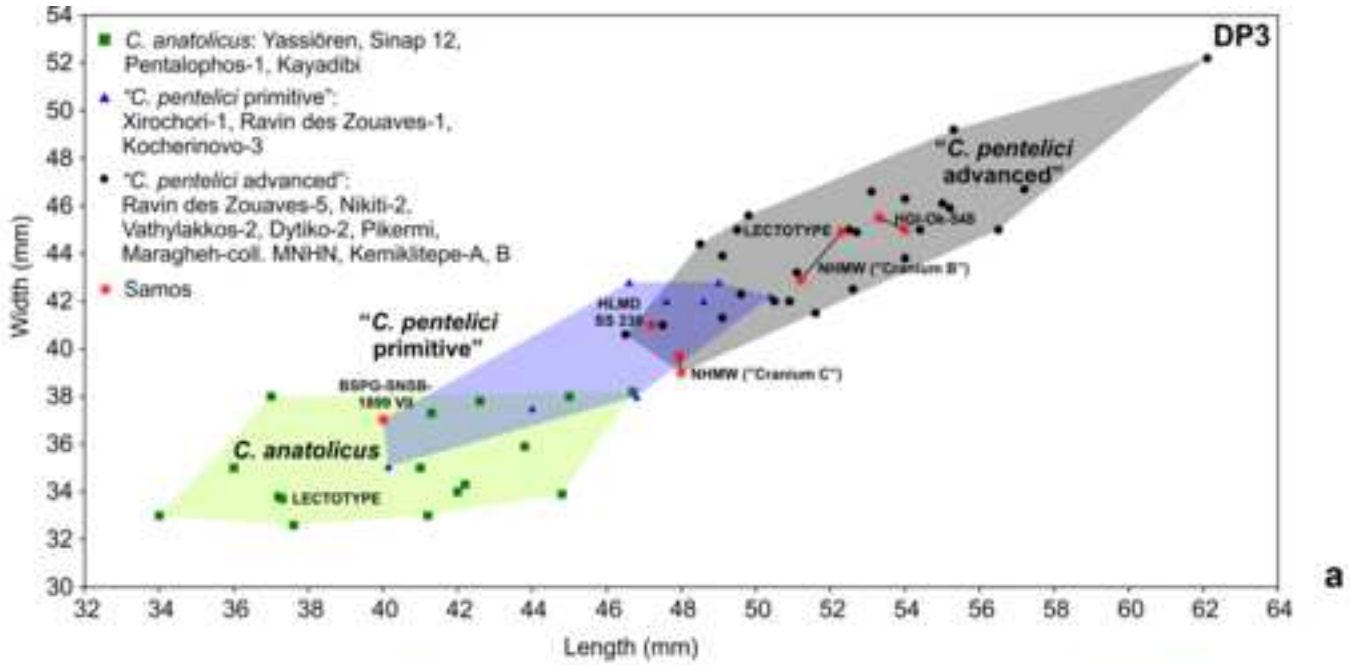
DP3
C. anatolicus: Yassiören, Sinap 12, Pentalophos-1, Kayadibi
"C. pentelici primitive": Xirochori-1, Ravin des Zouaves-1, Kocherinovo-3
"C. pentelici advanced": Ravin des Zouaves-5, Nikiti-2, Vathylakkos-2, Dytiko-2, Pikermi, Maragheh-coll. MNHN, Kemäklitepe-A, B
Samos
"C. pentelici advanced"
"C. pentelici primitive"
C. anatolicus
LECTOTYPE
NHMW ("Cranium B")
NHMW ("Cranium C")
HLMD SS 238
BSPG-SNSB-1899 V3
Width (mm)
Length (mm)
a

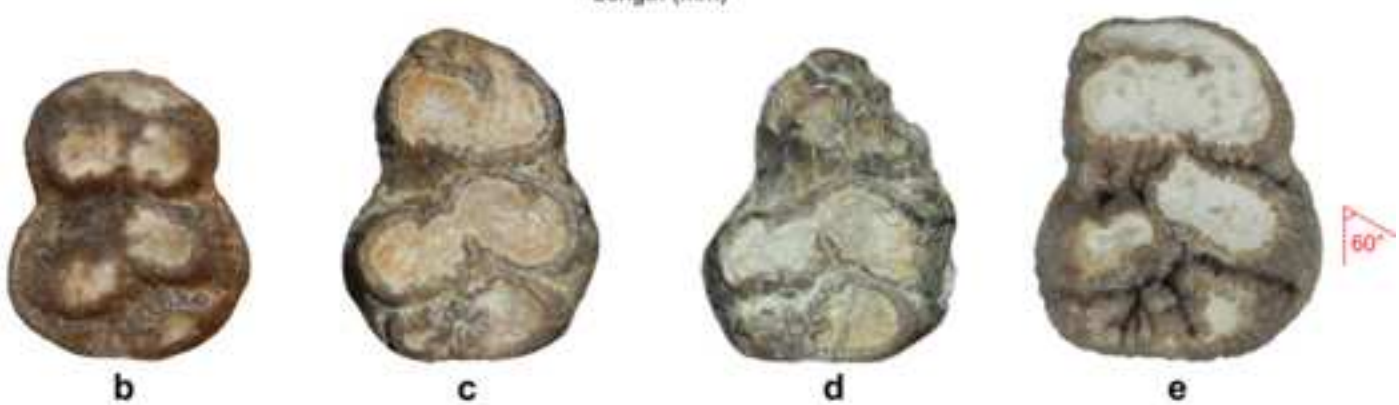
60°
b
c
d
e

1 cm

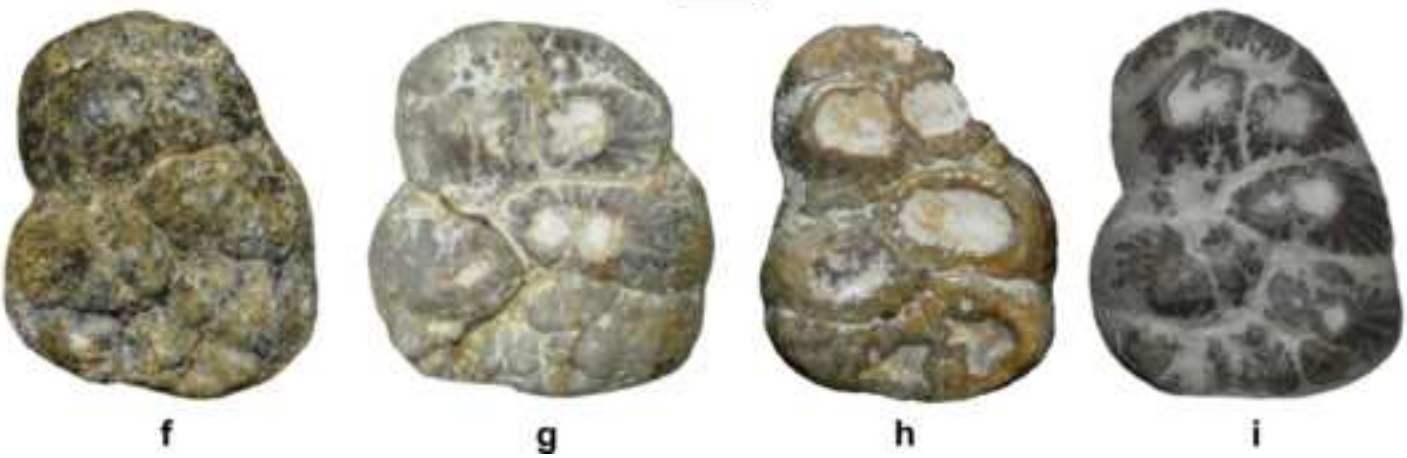
f
g
h
i

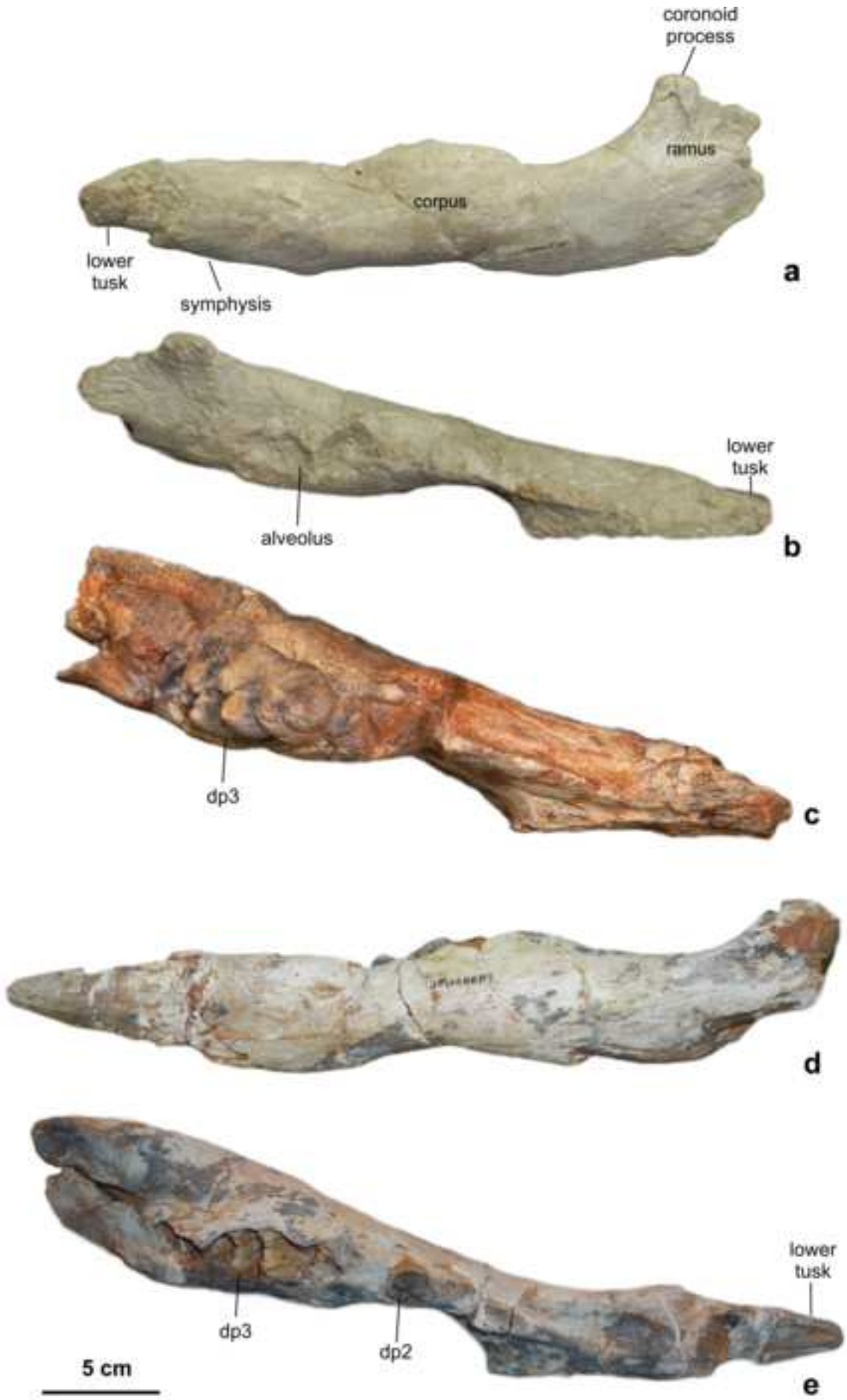
coronoid process
ramus
corpus
lower tusk
symphysis
a
lower tusk
alveolus
b
dp3
c
d
lower tusk
dp3
dp2
5 cm
e

Cranial measurements	*Deinotherium* SMF-M 3604	*Choerolophodon* SMF-M 3603
preserved length	400	430
length of premaxilla	-	250
length of fossa incisiva	-	225
length of nasal bones upon the nasal fossa	-	25
maximal supra-orbital width	-	264
anterior rostral width	-	141
width of nasal bones upon the nasal fossa	-	44
width of nasal fossa	-	105
length of zygomatic arch from the processus zygomaticus of the maxilla to the posterior border of the glenoid fossa	-	235
length of orbitotemporal fossa at the level of the zygomatic arch	-	109
palatal length from the root of DP2 to the choanae	-	174
thickness of processus zygomaticus of the maxilla	-	82
maximal width of choanae	39	37
internal maximal width of the palate	80	48
external maximal width of the palate	183	111
internal width of the palate	64	44
minimal palatal width between the interalveolar cristae	-	42
height of premaxilla	-	45
height of maxilla ventral to the processus zygomaticus	-	67
height of orbit	75	100
facial length from tip of the rostrum to the pterygoid process	-	360
length of orbitotemporal fossa	-	105

Mandibular measurements	*Deinotherium* SMF-M 3604
preserved length	430
symphyseal length	100
alveolar distance	222
ventral length from the gonion to the tip of the symphysis	360
maximal width	245
mandibular width at the root of ascending rami	237
width of horizontal ramus at the root of the ascending branch	100
width of horizontal ramus infront of the anterior deciduous premolar	64
posterior symphyseal width	140
anterior symphyseal width	60
maximal symphyseal width	140
minimal symphyseal width	60
maximal width of the rostral trough	56
minimal width of the rostral trough	38
internal width between the anterior deciduous premolars	59
maximal height of horizontal ramus	104
height of horizontal ramus at the root of the ascending branch	80
rostral height at the symphyseal border	91
rostral height at tip of rostrum	65
depth between gonion and coronoid process	110
mid-alveolar length	177

Choerolophodon SMF-M 3603
370
(63)
211
300
-
-
65
43
-
-
-
-
-
-
-
77
67
-
36
105
-

Species	Tooth	Inventory number	Side	L	W1	W2	W3
Deinotherium proavum	dp2	SMF-M 3604	dex	33.9	23.7	30.1	
			sin	33.8	23.0	30.2	
	dp3		dex	63.9	37.9	44.5	
			sin	64.1	39.1	43.9	
	dp4		dex	90.3	48.8	51.0	58.0
			sin	89.4	48.5	50.4	56.4
	DP2		dex	53.9	43.3	47.1	
			sin	53.1	42.2	45.9	
	DP3		dex	61.6	57.2	60.9	
			sin	64.2	56.7	64.7	
	DP4		dex	90.0	68.5	65.2	67.4
			sin	91.2	63.7	64.3	68.6
	dp3	MGL-S 1048	dex	57.6	35.0	42.3	
	dp4	MGL-S 381	sin	85.3	-	-	(51.0)
Choerolophodon pentelici	dp3	MGL-S 340	dex	57.3	24.0	33.2	
	dp4	MGL-S 333	dex	78.5	37.0	42.7	(46.7)
			sin	(76.0)	(36.7)	(43.2)	46.7
	m1		sin	-	48.8	-	-
	dp3	SMF-M 3603	dex	54.0	23.0	32.0	
	dp4		dex	-	36.7	-	-
	DP4		dex	(58.7)	44.0	-	-
			sin	(62.1)	44.5	-	-
	DP2	MGL-S 614	dex	33.7	18.5	24.0	
	DP3	HLMD-SS 230	dex	47.2	32.9	41.0	
			sin	(45.9)	-	41.8	
	DP4		dex	73.6	48.3	50.3	50.7
			sin	73.1	48.0	53.1	51.7